Explosive Ocean Island Volcanism Explained by High Magmatic Water Content Determined Through Nominally Anhydrous Minerals

Harri Geiger[1,2] , **Franz Weis**[2,3,4], **Valentin R. Troll**[2,4,5] , **Frances M. Deegan**[2,4] , **Henrik Skogby**[3] , **and Juan Carlos Carracedo**[5]

[1]Institute of Earth and Environmental Sciences, University of Freiburg, Freiburg im Breisgau, Germany, [2]Department of Earth Sciences, Natural Resources & Sustainable Development (NRHU), Uppsala University, Uppsala, Sweden, [3]Swedish Museum of Natural History, Department of Geosciences, Stockholm, Sweden, [4]Centre of Natural Hazards and Disaster Sciences (CNDS), Uppsala University, Uppsala, Sweden, [5]Universidad de Las Palmas de Gran Canaria, Instituto de Estudios Ambientales y Recursos Naturales (i-UNAT), Las Palmas de Gran Canaria, Spain

Abstract Ocean island basalt (OIB) magmas are generally water poor and usually contain less than 1 wt.% of H_2O. Explosive eruption styles are therefore rare. When explosive eruptions occur, they are thought to be driven by either volatile-enriched mantle sources or by gas segregation processes during magma differentiation. Here we report on crystal- and water-rich porphyritic basanites and ankaramites from El Hierro in the Canary Islands, Spain, that erupted inside the El Golfo giant landslide collapse embayment that formed at ≥39 ka. Using rock and mineral chemistry in combination with H_2O contents of nominally anhydrous minerals (olivine and clinopyroxene), we show that despite their relatively primitive composition, the post-collapse ankaramites are not primary mantle melts. Instead, they record high crystal contents as well as unusually high water contents of up to 3.20 ± 0.64 wt.% H_2O, and likely represent a normally inaccessible snapshot of dense crystal-rich magma compositions that reside in the sub-island underplating zone. We hypothesize that their eruption was facilitated by sudden decompression from crustal unloading, implying that the El Golfo landslide may have affected the deeper portions of the plumbing system and triggered the ascent of volatile-rich, crystal-laden magmas from the underplating zone. We propose that some "wet" and explosive ocean island eruptions might result from the ascent of deep-seated water-rich magmas in the aftermath of vertical unloading and associated decompression.

Plain Language Summary Volcanic eruptions on ocean islands are commonly of non-explosive character. However, violent explosive eruptions occasionally occur, but their underlying causes are poorly understood. El Hierro Island, Canary archipelago, experienced several giant landslides in its geological past, and after the most recent collapse some ~39k years ago, explosive volcanic activity commenced for a limited period of time. The explosive eruption products contain uncommonly crystal-rich volcanic rock fragments, and we find that pyroxene crystals contained in these eruptive products show that the host magmas were unusually water-rich and ascended from deep storage levels. We suggest that explosive eruptions on ocean islands can be triggered by landslide events and the associated decompression, allowing eruption of water and crystal-rich magmas that usually stay "hidden" in the underplating zone beneath the island, as their physical properties are not suitable for eruption without additional driving forces.

1. Introduction

The style of volcanic eruptions is strongly linked to the composition and volatile content of the pre-eruptive magma. Generally, higher contents of volatile compounds, such as water, carbon dioxide and sulfur species, usually cause more violent eruptions (e.g., Cashman, 2004; Dingwell, 1996; Sides et al., 2014). Ocean island volcanism is generally characterized by relatively water-poor and dominantly mafic magmas that contain ~1 wt. % H_2O and erupt in non-explosive fashion (Dixon & Clague, 2001; Dixon et al., 1997; Gurenko & Schmincke, 2000; Kovalenko et al., 2007; Moore, 1970; Simons et al., 2002; Wallace, 1998a, 1998b; Weis et al., 2015). Explosive basaltic eruptions nevertheless occasionally occur on ocean islands, as observed at Kīlauea (Hawaii; e.g. Houghton & Gonnermann, 2008; Sides et al., 2014) as well as evident from pyroclastic deposits and recent volcanic events on the Canary Islands (Spain, e.g. Carracedo et al., 2022; Longpré et al., 2009) and the Cape Verde archipelago (DeVitre et al., 2023). Despite their increasing recognition, the underlying causes for explosive ocean island volcanism are not yet widely understood and explosive basaltic eruptions have been

considered to result either from shallow crustal volatile enrichment during magma storage and differentiation (Cashman, 2004), or, as recently suggested for Kīlauea and the Cape Verdes, from volatile-rich primary mantle melts and associated rapid magma ascent (Sides et al., 2014, DeVitre et al., 2023).

El Hierro is a relatively young Atlantic ocean island belonging to the Canary Archipelago located ca. 450 km off the west coast of North Africa that experienced explosive basaltic volcanism in its geological past (Carracedo et al., 2001; Carracedo & Troll, 2016; Guillou et al., 1996; Schmincke, 1982). Following a lateral collapse of the island's flank between 87–39 ka, extensive crystal-rich basanites (petrographically known as ankaramites with clinopyroxene>olivine) erupted from numerous vents within the resulting El Golfo embayment and on the crest of the landslide structure (Carracedo & Troll, 2016; Manconi et al., 2009). The erupted products predominantly comprise lava flows but also ash and lapilli deposits that contain large crystal-rich volcanic bombs, pointing to explosive behavior as an integral part of the post-collapse volcanism on El Hierro (Figures 1 and 2). It has previously been suggested that these post-collapse eruptions tapped a deep magma reservoir due to rapid unloading as a result of the El Golfo giant landslide (cf. Longpré et al., 2011; Manconi et al., 2009; Masson, 1996) and a similar process has been suggested for Tenerife Island, where rift unloading events were proposed to have disrupted magma plumbing and facilitated emplacement of ankaramite lava and dykes (Carracedo et al., 2011; Carracedo & Troll, 2013; Deegan et al., 2012; Longpré et al., 2009). Such unloading effects are not instantaneous, but have been shown to last for up to 50 ka after a collapse event, implying that changes in magma composition and plumbing system readjustment operate for some time after the actual unloading event (Carracedo et al., 2011; Cornu et al., 2021, DeVitre et al., 2023).

Magmatic underplating has been recognized as a significant contributor to ocean island evolution over the last two decades (e.g., Carracedo, Troll, et al., 2015; Hansteen et al., 1998; Klügel et al., 2015) and has recently been suggested to represent the most significant process in ocean island growth (Carracedo, Troll, et al., 2015; Klügel et al., 2015). Geophysical measurements during and after the 2011–2012 eruption of El Hierro determined a vertical ground displacement (i.e., island uplift) of as much as 22 cm (Carracedo, Troll, et al., 2015; Gonzalez et al., 2013), while the eruptive volume was comparatively minor (Rivera et al., 2013). This observation is direct evidence for island growth via underplating and implies considerable magma influx and storage at upper mantle depth to promote vertical growth of the entire island. The realization that OIB melts can become enriched in volatiles in such underplating zones is consistent with the occurrence of amphibole xenocrysts and amphibole cumulate nodules in Canary basanite magmas (e.g., Barker et al., 2015; Brey & Schmincke, 1980; Carracedo & Troll, 2016; Neumann et al., 2000), and points toward the existence of extensive hydrous cumulates under the Canary Islands. Stagnation, evolution and volatile enrichment of mantle-derived magma in underplating zones may thus facilitate the possibility of explosive eruptive behavior on ocean islands, especially during and after vertical unloading events (see e.g. Longpré et al., 2009).

To improve our understanding of the relationship between vertical unloading effects, readjustment of plumbing systems, and magmatic volatile contents on ocean islands (cf. Amelung & Day, 2002), we measured water contents in nominally anhydrous clinopyroxene and olivine phenocrysts from ankaramite lava and lava bombs erupted from post-collapse vents within the El Golfo embayment using Fourier Transformed Infrared Spectroscopy (FTIR). The H_2O content of the post-collapse magmas was determined by applying calculated water partition coefficients for clinopyroxene and olivine (e.g., Nazzareni et al., 2011; O'Leary et al., 2010; Wade et al., 2008; Weis et al., 2015). We find that clinopyroxene water contents in post-collapse ankaramite lava bombs are unusually high for OIB magmas and that the corresponding magmatic H_2O contents correlate with geochemical fractionation indices. We therefore advocate for the presence of a water-rich, upper mantle underplating zone where magmas reside and fractionate beneath El Hierro prior to ascent and eruption.

2. Geological Background

El Hierro is the westernmost and youngest of the Canary Islands (<1.2 Ma; Figures 1a and 1b) and its eruption products are dominantly basaltic in composition (Carracedo & Troll, 2016; Guillou et al., 1996; Zaczek et al., 2015). The island is currently in its shield stage of growth and its stratigraphy can be divided into three main geological units (Carracedo et al., 2001; Carracedo & Troll, 2016). These are from oldest to youngest: the Tiñor volcano, the El Golfo volcano, and the recent (post El Golfo) rift volcanism (Carracedo, 1994, 1999; Carracedo et al., 2001). Four major landslides have been recorded during the island's geological evolution, comprising the Tiñor, the El Julán, the Las Playas, and the El Golfo giant collapses (Figure 1b), and the resulting landslide
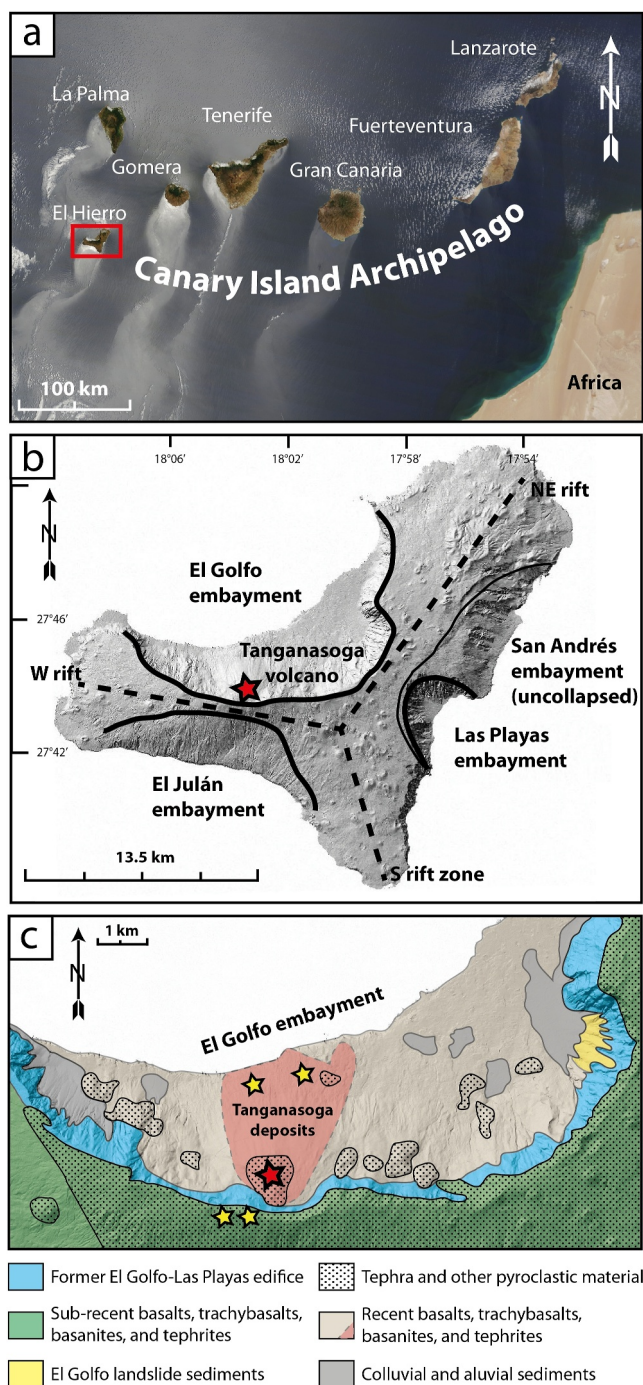
Figure 1. (a) Satellite map showing the location of El Hierro in the Canary archipelago (red box; Carracedo & Troll, 2016). (b) Overview DEM map of El Hierro showing the three main rift zones of the island (stippled lines) and the main landslide embayments (solid lines) DEM source: GRAFCAN (2024). The Tanganasoga volcano is a prominent feature located inside the El Golfo landslide embayment and is marked with a red star. (c) Simplified geological map of the El Golfo collapse embayment showing the distribution of different volcanic rocks and pyroclastic material. Ankaramite samples were collected from pyroclastic deposits on the rift zone above the El Golfo embayment and from lava directly within the embayment. Sampling locations are marked with yellow stars (DEM source: GRAFCAN (2024)).
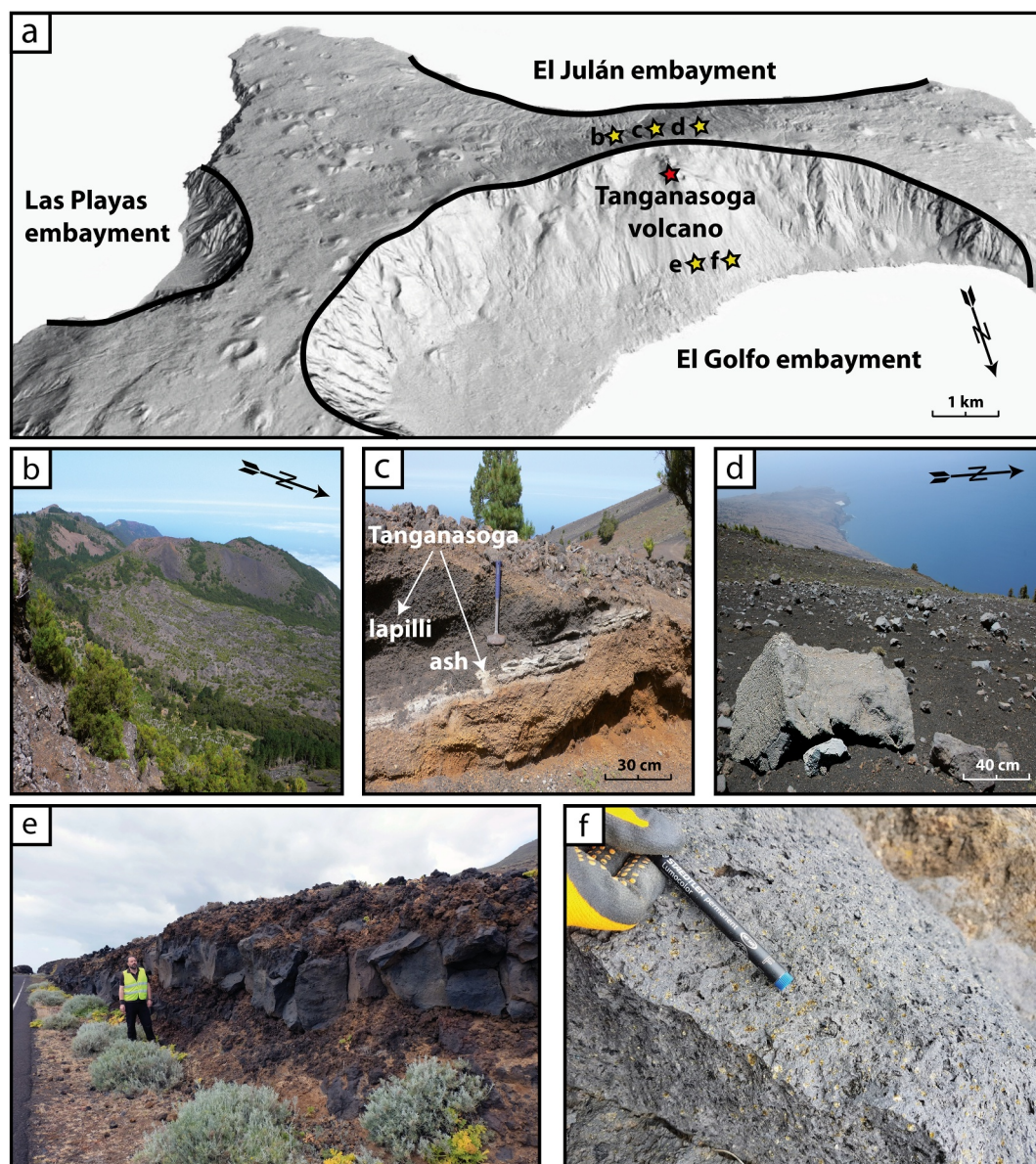
Figure 2. (a) Oblique view of the El Golfo collapse embayment (Source: GRAFCAN (2024)). Photo locations of panels (b) to (f) are indicated by yellow stars, the Tanganasoga volcano is indicated by a red star. (b) Summit vent of Tanganasoga and post-collapse ankaramite lava flows viewed from the rift zone crest above the volcano. (c) Layers of pyroclastic material on the rift above the Tanganasoga edifice. (d) Ankaramite blocks and ash deposits erupted from Tanganasoga volcano that were deposited on the crest of the rift zone. (e and f) Example of an ankaramite lava flow on the northwestern flank of the Tanganasoga edifice with exceptionally high contents of large clinopyroxene and olivine crystals.

embayments define the island's steep topography to this day (Carracedo, 1994; Day et al., 1997; Gee et al., 2001; Masson et al., 2002). The El Golfo collapse is the youngest giant landslide in the whole of the Canary Islands and has been only partially infilled with lava from post-collapse vents that developed within the collapse embayment and from the active rift zone above (e.g., Carracedo et al., 2001; Carracedo & Troll, 2016; Longpré et al., 2011; Manconi et al., 2009; Figure 1c). The associated debris avalanche removed 150–180 km^3 of volcanic rock from the island's flank, leaving a large field of blocky volcanic debris on the submarine slopes of El Hierro (Carracedo & Troll, 2016; Masson, 1996).

The oldest exposed formation on El Hierro is the Tiñor shield volcano (1.2–0.88 Ma), which collapsed northward to produce the Tiñor embayment. This embayment was filled by eruptive products of the subsequent El Golfo

volcano (0.88–0.16 Ma; Guillou et al., 1996). At ~0.6 Ma, the southwestern flank of the El Golfo volcano collapsed, producing the giant El Julan landslide. This event was later followed by the Las Playas landslide on the eastern side of the island (~145 ka), which remains unstable to this day in the form of the San Andrés fault system (Day et al., 1997; Masson et al., 2002). Eventually, the El Golfo volcano itself collapsed to the Northeast between ~87 and 39 ka, resulting in submarine avalanche deposits and forming the enormous El Golfo landslide depression (Carracedo et al., 2001; Gee et al., 2001; Longpré et al., 2011; Masson, 1996; Masson et al., 2002). At around 158 ka, during the terminal stages of the El Golfo volcano but prior to the El Golfo landslide, rift volcanism commenced on the island (Guillou et al., 1996). Three active rift zones developed around the main landslide scars, which continue to be active today (Figure 1b). The active rift zones show tightly grouped emission vents and volcanism on the rifts that is largely comprised of effusive lava flows and scoria deposits emitted from fissure-fed strombolian cinder cones (Carracedo et al., 2001; Guillou et al., 1996; Figure 1b). Erupted products from the rift zones have partly filled the El Julán, Las Playas, and El Golfo embayments, with lava compositions being mainly mafic alkaline and ranging from picrobasalt to basanite (Carracedo et al., 2001, 2011; Stroncik et al., 2009). Historic volcanic activity on El Hierro is restricted to an alleged but unconfirmed eruption at Lomo Negro in 1793 and the 2011–2012 submarine eruption near La Restinga off the southern tip of the island (Carracedo, Troll, et al., 2015; Carracedo et al., 2012; González et al., 2013; Guillou et al., 1996; Hernández Pacheco, 1982; Zaczek et al., 2015).

Among the post-collapse vents in the El Golfo embayment, the Tanganasoga volcano is the most prominent edifice with a minimum age of 8,000 years (Pellicer, 1977; Perez-Torrado et al., 2011; Figures 1b and 1c & 2). The relatively primitive post-collapse magmas were previously interpreted to be the result of upper-mantle decompression due to unloading after the giant El Golfo landslide (Carracedo et al., 2001; Guillou et al., 1996; Manconi et al., 2009). Indeed, giant landslides have been shown to cause pressure changes exceeding 1 MPa at upper mantle depth, promoting dense and volatile-rich primitive magmas to ascend at higher than normal rates (cf. Cornu et al., 2021; Manconi et al., 2009; Pinel & Jaupart, 2005).

3. Methods

3.1. Sample Collection and Preparation

The rock samples examined in this study comprise ankaramite lava flows and lava bombs that were collected on the crest of the El Golfo embayment, just southeast of the Tanganasoga edifice, as well as on the northwestern flank of the Tanganasoga edifice within the El Golfo embayment itself (Figures 1c and 2). The rock samples were crushed and suitable clinopyroxene and olivine crystals larger than ≥300 μm in size were hand-picked under a binocular microscope from the crushed material and prepared for FTIR spectroscopy and electron probe microanalysis (EPMA). A portion of each rock sample was also used to prepare polished thick sections for EPMA, while another aliquot was powdered for major element analysis using an automated agate mortar grinder (Retsch RM200) at the Department of Earth Sciences, Uppsala University, Sweden. One set of clinopyroxene crystals ($n = 44$) were oriented along the crystallographic c-axis by crystal morphology and optical microscopy and polished on their (100) and (010) crystal faces, on which the directions of the main refractive indices (α, β, and γ) occur. Another crystal set of clinopyroxene ($n = 51$) and all olivine crystals ($n = 74$) were polished unoriented on two parallel sides for unpolarized FTIR measurements. Various sandpaper grades were used to grind and polish the crystals to a thickness of a few hundred micrometers. For EPMA of clinopyroxene and olivine, a subset of crystals selected for FTIR analysis were chosen, totaling 39 clinopyroxene and 61 olivine crystals.

3.2. Whole-Rock and Mineral Composition

A small number of whole-rock samples were analyzed for major and trace elements. These include five samples at Acme Analytical Labs Ltd in Vancouver, and four samples at Activation Laboratories Ltd in Ontario, Canada. In both labs, major elements were measured by Inductively Coupled Plasma Optical Emission Spectrometry (ICP-OES). Sample preparation included mixing of powdered rock material with a $LiBO_2/Li_2B_4O_7$ flux before sample fusion in a furnace. Before measurement, the sample bead was dissolved by applying dilute nitric acid digestion. The iron content is reported as Fe_2O_3. Data quality was monitored using a set of certified, internal reference materials (e.g., NIST, USGS, OREAS). Trace and rare earth elements were analyzed by Inductively Coupled Plasma-Mass Spectrometry (ICP-MS) after preparation by multi-acid digestion. Uncertainties are estimated to be

<0.2% for SiO_2, Al_2O_3, Fe_2O_3, MgO, CaO, Na_2O, K_2O, TiO_2, P_2O_5, MnO, and Cr_2O_3 and <4% (2 s.d.) for most trace and REE elements.

Major element compositions of clinopyroxene, olivine, and groundmass in polished thick sections were acquired with a Field Emission-EPMA JXA-8530F JEOL hyperprobe at the Department of Earth Sciences, Uppsala University, Sweden. Between 5 and 8 spots were analyzed on each crystal using a beam diameter of 1 µm, with a beam current of 10 nA and an acceleration voltage of 15 kV with counting times of 10 s on peak and 5 s on lower and upper background. Standards for calibration used were fayalite (Fe_2SiO_4) for Fe, periclase (MgO) for Mg, pyrophanite ($MnTiO_3$) for Mn and Ti, corundum (Al_2O_3) for Al, wollastonite ($CaSiO_3$) for Ca and Si, eskolaite (Cr_2O_3) for Cr, nickel oxide (NiO) for Ni as well as albite ($NaAlSi_3O_8$), orthoclase ($KAlSi_3O_8$) and apatite $Ca_5(PO_4)_3(OH,F,Cl)$ for Na, K and P, respectively.

Several of the analyzed clinopyroxene crystals showed weak patchy zonation in backscattered electron (BSE) images, pointing to dynamic magma ascent processes. Therefore, for each crystal an average composition was additionally calculated from all analyzed spots. A detailed description of the EPMA procedure and the analytical uncertainties are presented in Barker et al. (2015). From the obtained weight percentages, the number of atoms per formula unit in each crystal was calculated on the basis of three or four cations. The amount of Fe_2O_3 and FeO for whole rock analyses was determined by applying a ratio of 0.21 for Fe^{3+}/Fe_{total} (see Geiger et al., 2016).

In addition, groundmass composition was obtained by EPMA using a defocused beam (20 µm) and measuring over a grid of 120×120 µm. The analyzed areas were chosen by sample homogeneity and size of visible crystals, that is, avoiding larger crystals. For each rock sample, two grids were analyzed and an average value was calculated from all the obtained analyses. All analytical results are reported in Supporting Information S1.

3.3. Fourier-Transform Infrared (FTIR) Spectroscopy

The water contents in the olivine and clinopyroxene phenocrysts were measured by FTIR spectroscopy following the approach of Weis et al. (2016). Polarized IR spectra in the range 2,000–5,000 cm^{-1} were acquired on the oriented clinopyroxene crystals along the directions of the main refractive indices (α, β, and γ) in order to obtain the total absorbance: $A_{total} = A_\alpha + A_\beta + A_\gamma$. The polished crystals were analyzed at the Swedish Museum of Natural History in Stockholm using a Bruker Vertex 70 spectrometer equipped with an NIR source (halogen lamp) and a CaF_2 beamsplitter, coupled to a Hyperion 2000 microscope with a ZnSe wiregrid polarizer and an InSb detector. The crystal thickness varied between 300 and 800 µm, with most crystals having a thickness between 400 and 700 µm for both the (100) and (010) orientation. Cracks and inclusions in the crystals were avoided by applying small apertures (100–400 µm) for masking during analysis. However, in some cases impurities were present in the beam path but these appeared to not have had any significant effect on the OH range of the spectra. For each individual spectrum, 128 scans were performed on each crystal and then averaged. The obtained spectra were baseline corrected by a polynomial function and the OH bands were fitted with the software PeakFit. The corresponding water contents were then calculated using the calibration function established by Libowitzky and Rossman (1997), which has previously been used successfully for synthetic as well as natural clinopyroxene samples (e.g., Sundvall & Stalder, 2011) and which was reconfirmed by Mosenfelder and Rossman (2013).

In addition to polarized measurements, water contents in clinopyroxene and olivine were obtained using the method described by Kovacs et al. (2008), which uses non-polarized measurements of unoriented, double-sided polished crystals. Thicknesses varied between 200 and 400 µm for clinopyroxene and 600 and 1,100 µm for olivine. The method relies on a statistical approach and requires the analysis of at least 10 crystals to constrain analytical uncertainty. Corresponding water contents were again determined by applying the calibration by Libowitzky and Rossman (1997), which is most suitable when unpolarized measurements are applied (Libowitzky & Rossman, 1996). This calibration was also confirmed to give similar results as mineral specific-calibrations for olivine (e.g., Withers et al., 2012).

Six melt inclusions within olivine crystals were analyzed for their water content by performing unpolarized measurements with the same spectrometer system. The olivine crystals were polished on opposite sides until a flat surface of the inclusion was achieved on either side. The melt inclusions showed the typical OH-bands in volcanic glass with the typical broad and asymmetric band centered at 3,530 cm^{-1}, corresponding to the contributions of both OH^- and molecular H_2O stretching vibration in the glass as well as the stretching/bending combination

mode for OH^- at 4,500 cm^{-1} (cf. Okumura et al., 2003; Von Aulock et al., 2014). For quantification, the maximum absorption of the main OH-band at 3,530 cm^{-1} and a molar absorption coefficient of 63 ± 3 L/mol-cm was used (after Wallace, 1998a).

Potential uncertainties for calculated water contents can arise from baseline correction and measurements of crystal thickness. However, due to the quality of the spectra and the relatively large thickness of the crystals a maximum error of ±10% is assumed for the precision of the calculated clinopyroxene water contents. In addition, the uncertainty associated with the calibration of the absorption coefficients is ±10% (cf. Libowitzky & Rossman, 1997), resulting in an overall uncertainty of ±20% for the calculated clinopyroxene water contents from polarized measurements. The error for unpolarized measurements is slightly higher, with a precision of ca. ±20%, thus raising the total uncertainty to ±30% (Kovacs et al., 2008). The maximum uncertainty for the water content in melt inclusions is estimated to be less than ±20% due to a small error in the absorption coefficient (cf. Wallace, 1998a) and the good quality of the spectra.

3.4. Magmatic Water Content Calculation

Initial magmatic water contents were calculated using the obtained clinopyroxene water contents and mineral compositional data, as well as currently available partition coefficients for water between clinopyroxene and basaltic melt. The calculations were performed by applying the formula in O'Leary et al. (2010) for the calculation of partition coefficients ($\ln_D = -4.2(\pm0.2) + 6(\pm0.5)^{VI}[Al^{3+}] - 1(\pm0.2)[Ca^{2+}]$), which considers the amount of tetrahedral aluminum that is strongly interlinked with the hydrogen incorporation into clinopyroxene due to charge balancing processes. Since geochemical data to determine $^{VI}[Al^{3+}]$ was not obtained for each individual clinopyroxene crystal that was also analyzed by FTIR, an average value was calculated from the available data which showed very little to almost no variation compared to the whole sample set. Similarly, magmatic water contents were calculated based on water contents in olivine and using the formula for partition coefficients by Le Voyer et al. (2014).

3.5. Olivine Diffusion and Ascent Rate Calculation

In order to test for a hydrogen diffusion profile in olivine, the water content in two larger olivine crystals from sample T1 was measured in more detail from core to rim. The crystals were prepared in the same way as other olivine crystals for FTIR analysis and unpolarized FTIR measurements. The diffusion of hydrogen represented by the IR-absorption at a given point (A_d) on the crystal over the initial absorption (A_{in}) in the center of the crystal can be fitted to a diffusion curve based on Fick's second law and various time intervals. The time for which diffusion was active in the crystal could therefore be determined. For the fitting process, experimentally derived diffusion data presented in Demouchy and Mackwell (2003) as well as the temperature from our thermobarometry calculations (see below) were applied. Since the olivine in this study is Fe-poor, hydrogen diffusion via vacancy diffusion (i.e., defect resetting) is assumed to be the driving factor for the hydrogen diffusion (cf. Tian et al., 2017) instead of the Fe redox-reaction. After determining the time for diffusion activity, an ascent rate was calculated for the magma using the depth determined by thermobarometry modeling. The total error for the absorption ratios is ±20%, despite unpolarized measurements, since the error for the absorption coefficients is equaled out.

3.6. Clinopyroxene-Melt Thermobarometry

Groundmass and non-averaged clinopyroxene compositional data were used to calculate crystallization pressures and temperatures by applying a suitable mineral-melt thermobarometer based on jadeite-diopside/hedenbergite exchange equilibria between clinopyroxene and coexisting melt (e.g., Neave & Putirka, 2017; Putirka, 2008; Putirka et al., 1996, 2003). More specifically, we used the most recent recalibration of Eq. 30 in Putirka (2008) by Neave and Putirka (2017) for pressure and Eq. 33 in Putirka (2008) for temperature. Both of these are currently the most precise clinopyroxene-melt models for pressure and temperature, respectively, with standard errors of estimate (SEE) of 140 MPa and 45°C, and are calibrated for hydrous and anhydrous systems (Neave & Putirka, 2017).

Equilibrium between clinopyroxene and their associated melt is a prerequisite for robust pressure and temperature estimation. A first equilibrium test evaluates if clinopyroxene-melt couples fall into the $K_{D(Fe-Mg)} = 0.28 \pm 0.08$ exchange coefficient envelope. As the first test can sometimes lead to erroneous equilibrium assumption (cf. Neave & Putirka, 2017), a second test comparing predicted versus observed clinopyroxene exchange components

(e.g., CaTs, EnFs, DiHd, Jd) on a one-to-one line (within ±0.05) is required. Clinopyroxene-melt couples that pass both tests are assumed to be in equilibrium and can be used for thermobarometry calculations (see Supporting Information S1 for full procedure).

In addition, the clinopyroxene-melt thermobarometry model used here requires the input of a melt composition and H_2O concentration. Possible melt compositions can be provided by whole rock and groundmass analyses, while H_2O concentration is taken from magmatic water calculations in this study. The whole rock compositions employed here have an average Mg# of 29.71 and an average MgO content of 9.56 wt%, while the groundmass compositions have an average Mg# of 43.10 and an average MgO content of 5.21 wt% (see Supporting Information S1 for full data set). To convert pressures to depth, lithological densities are required. We employed a combined crustal and upper mantle density of 3,100 kg/m^3 (cf. Tenzer et al., 2013) for pressure to depth conversion.

4. Results

4.1. Petrography and Mineral Chemistry

Post-collapse lava and lava bombs are dark gray, porphyritic and highly vesicular ankaramites, which classify as basanites on the TAS diagram (Figures 2f and 3a). The main mineral phases are clinopyroxene, olivine, and various oxides, which together make up 50 vol.% crystal cargo set in a microlite-bearing, glassy groundmass (Figures 3b and 3d). Clinopyroxene crystals are usually <10 mm in size, euhedral to subhedral, and show dissolution textures and patchy zoning (Figure 3b). Compositionally, clinopyroxene have a range of $Wo_{49}En_{31}Fs_{17}$ to $Wo_{51}En_{34}Fs_{19}$, classifying them as titanium-rich diopside (~3.0 wt.% TiO_2; $n = 39$; after Morimoto et al. (1988); Figure 3c). Olivine phenocrysts are <5 mm in size, euhedral to subhedral and have a compositional range of Fo_{79}-Fo_{82} (average Fo_{80}, $n = 61$; after Brown (1980); Figures 3d and 3e). Clinopyroxene have Mg numbers between 77 and 80 (mean = 78), while olivine have Mg numbers between 78 and 81. The groundmass consists of microlites of plagioclase, pyroxene, olivine, various oxides, and smaller (<10 μm) domains of glass.

4.2. Major and Trace Element Geochemistry

On a total alkali versus silica diagram, El Hierro post-collapse ankaramites fall into the foidite and basanite fields, and thus can be labeled basanites based on the absence of foids as phenocryst phase. The samples therefore plot at the primitive end of the El Hierro lava compositional suite (Figure 3a). The compositions of our samples also overlap with the mafic end of the magmatic trends for La Palma and Tenerife, which, however, extend to more evolved compositions.

El Hierro post-collapse ankaramites plot, for the most part, along the liquid line of descent inferred for the El Hierro, La Palma, and Tenerife suites on MgO variation diagrams (Figures 4a–4e). While Al_2O_3, Na_2O, CaO, and Nb values for our ankaramites plot toward the more primitive end of the trend (Figures 4b–4d), TiO_2 shows elevated values for the El Hierro and Tenerife ankaramites as well as for parts of the El Hierro suite compared to La Palma and and other Tenerife volcanic rocks, possibly pointing to accumulation of Fe-Ti-Oxides (Figure 4a). Ni values of our El Hierro ankaramites as well as for Tenerife ankaramites also plot at higher values and hence point to a degree of olivine accumulation during petrogenesis (Figure 4f).

On a Nb/Y versus Zr/Y plot, the ankaramite samples of this study along with all other shown El Hierro, La Palma, and Tenerife rocks from the literature do not overlap with the established reference fields for normal mid-ocean ridge basalt (NMORB) and OIB (Figure 4g; after Fitton et al., 1997, 2003). Instead, our ankaramites as well as all literature data plot at distinctly higher Nb/Y and Zr/Y ratios, indicating that they are all the result of differentiation and accumulation rather than being primary mantle melts.

4.3. Water Contents Determined From Olivine, Clinopyroxene, and Melt Inclusions

Clinopyroxene and olivine, although being nominally anhydrous, incorporate small amounts of hydrogen in structural defects such as cation vacancies (e.g., Mg^{2+} vs. $2H^+$) and charge deficiencies (e.g., Si^{4+} vs. $Al^{3+} + H^+$) during growth from a hydrous magma. The hydrogen is bonded to oxygen as OH^-, which is regarded as an oxide component that can be expressed as water concentration (i.e., wt. ppm H_2O). Upon ascent, and during magma degassing, clinopyroxene will dehydrate by hydrogen diffusion, which follows the relatively fast but reversible
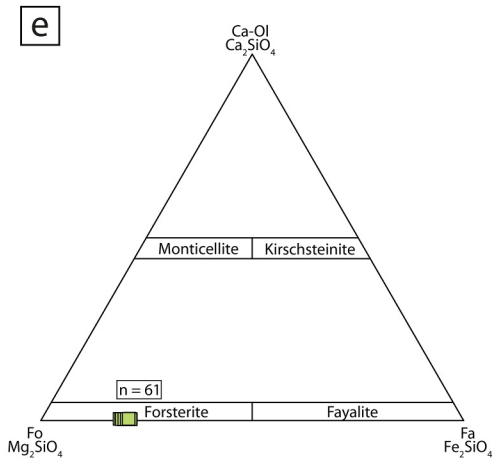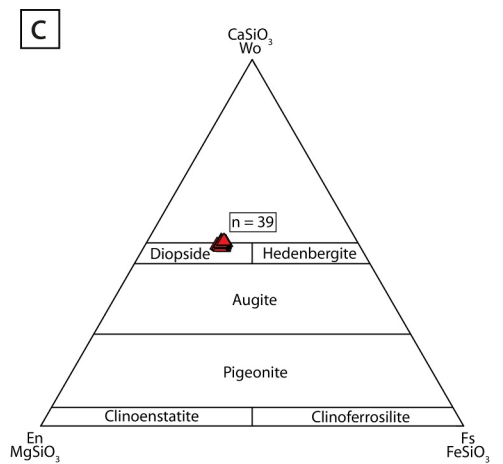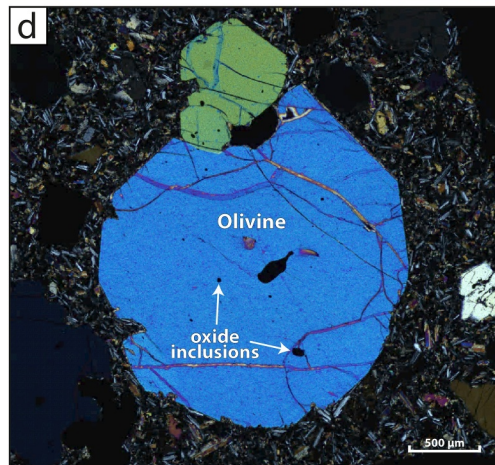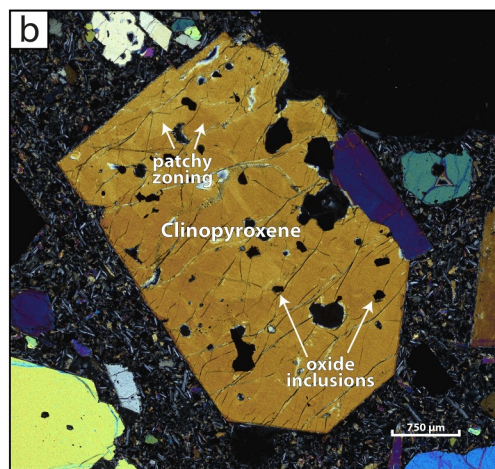
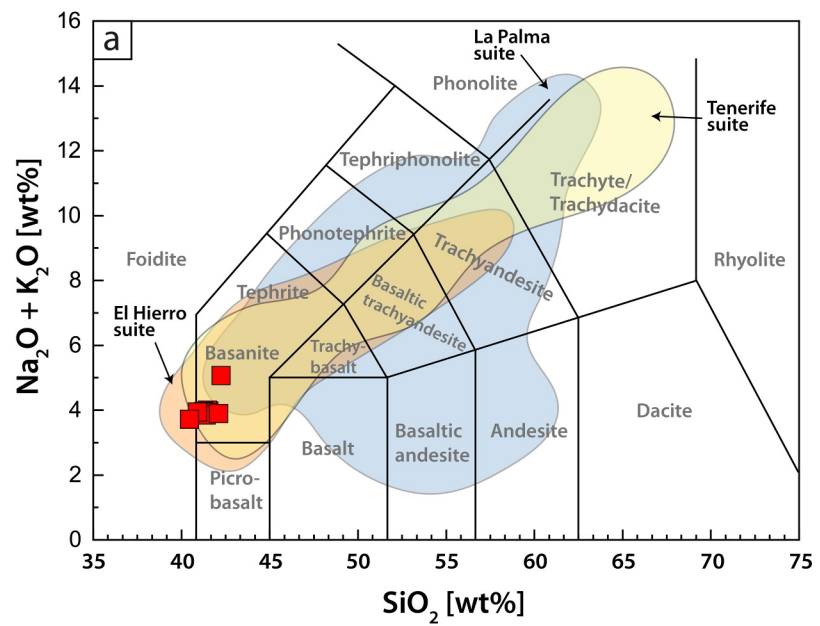**Figure 3.**

redox reaction $OH^- + Fe^{2+} \leftrightarrow O^{2-} + Fe^{3+} + \frac{1}{2} H_2$ (e.g., Skogby, 1994; Weis et al., 2015, 2016). For olivine, in turn, hydrogen loss is likely controlled by the diffusion of metal vacancies (e.g., Tian et al., 2017). At magmatic temperatures (i.e., ≥1000°C) diffusion profiles over distances of several millimeters may be produced within minutes in olivine and iron-rich clinopyroxene crystals (e.g., Woods et al., 2000). Therefore, rapidly transported and quickly cooled (quenched) explosive or chilled intrusive samples can preserve the original water contents, whereas lavas often show evidence of extensive dehydration during transport and slow cooling at the surface (e.g., Lloyd et al., 2016; Radu et al., 2023; Weis et al., 2015).

All analyzed clinopyroxene showed vibrational band peaks at 3,630, 3,530, and 3,460 cm^{-1} in the IR spectra that correspond to the typical vibrational bands expected for OH in diopside (Figure S2a in Supporting Information S1; Skogby, 2006). The OH band at around 3,630 cm^{-1} is strong when measured along the α and β directions, while the two bands around 3,530 and 3,460 cm^{-1} dominate along the γ direction. This infrared-pleochroic behavior is typical for clinopyroxene OH-bands and thus excludes the influence of possible OH-bearing impurities (Figure S2a in Supporting Information S1; cf. Beran, 1976). The unpolarized measurements resulted in a spectrum showing all three OH-bands combined (Figure S2a in Supporting Information S1). Clinopyroxene crystals ($n = 95$) show water contents ranging from 18 to 823 ppm (see Supporting Information S1 for full data set).

The unpolarized spectra obtained from olivine show OH-bands between 3,400 and 3,700 cm^{-1} and are typical for OH spectra in natural forsterite from basalts and mantle xenoliths globally (Figure 5b; e.g., Demouchy & Mackwell, 2006; Miller et al., 1987) Water contents in post-collapse olivine crystals ($n = 74$) range from below the detection limit to 18 ppm H_2O (see Supporting Information S1 for full data set), which is within the range of values observed for olivine pheno- and xenocrysts in basalts elsewhere (0–25 ppm H_2O; Peslier, 2010). A significant difference in water contents of olivine crystals in sample T4 compared to the other lava bomb samples, such as seen for clinopyroxene crystals, is not observed.

The analyzed melt inclusions showed the typical FTIR bands with the main band at 3,530 cm^{-1} (Figure S2c in Supporting Information S1). Water contents in the olivine-hosted melt inclusions range from 0.20 to 1.09 wt.% H_2O (see Supporting Information S1 for full data set).

The overall distribution of H_2O contents in olivine is more homogenous compared to clinopyroxene. In order to test for any diffusive hydrogen loss in olivine from ankaramite bombs, hydrogen profiles were measured rim to rim across two olivine crystals. No strong diffusion profiles could be identified in the two investigated olivine crystals (T1 Ol Dif 1 and 2). However, in T1 Ol Dif 2, a gradual decrease in water content can be seen from the center of the crystal to the margin, most likely representing metal vacancy diffusion during magma ascent. This diffusion profile can be used to fit a curve representing hydrogen diffusion in olivine for a certain temperature and time. We used the temperature estimate from our thermobarometry results (~1200°C) as input for T. At this temperature, logD for hydrogen diffusion is −10.4 (Demouchy & Mackwell, 2003). The profile observed in T1 Ol Dif 2 can be fitted to hydrogen diffusion lasting over 30 min (Figure 5). This time interval, in turn, together with an average crystallization depth of 18.5 km for the sample suggests an ascent rate of about 10.3 m/s. No curve can properly be fitted to the results of crystal T1 Ol Dif 1 and hence, the results cannot reliably be used for estimating an ascent rate.

4.4. Magmatic Water Content

To calculate partition coefficients between our clinopyroxene crystals and their parental melts, we used clinopyroxene compositional data and the equation of O'Leary et al. (2010); ($\ln_D = -4.2(\pm 0.2) + 6(\pm 0.5)^{VI}[Al^{3+}] - 1(\pm 0.2)[Ca^{2+}]$; see Methods). Since clinopyroxene crystals in the two lava flow samples underwent extensive hydrogen loss, they are not considered prime targets for primary magmatic water determination. Employing the aforementioned partition coefficients together with the clinopyroxene water contents from the ankaramite lava

Figure 3. (a) Total alkali versus silica (TAS) diagram for volcanic rocks from El Hierro, La Palma, and Tenerife. Post-collapse ankaramites from El Hierro (red squares, this study) classify as foidites and basanites and plot at the more primitive end of the El Hierro magmatic trend. All three magmatic trends overlap broadly and span a large compositional range from foidite to phonolite. Data for the El Hierro, La Palma, and Tenerife reference fields are from Carracedo et al. (2001, 2015a); Klügel et al. (2000); Rodríguez-Badiola et al. (2006). (b) Euhedral clinopyroxene crystal with visible patchy zoning and oxide inclusions under cross-polarized light (XPL). (c) Clinopyroxene from post El Golfo collapse ankaramites classify as diopsides ($n = 39$). (d) Subhedral olivine crystal with oxide inclusions in XPL. (e) Compositions of post-collapse olivine, which classify as forsterite.
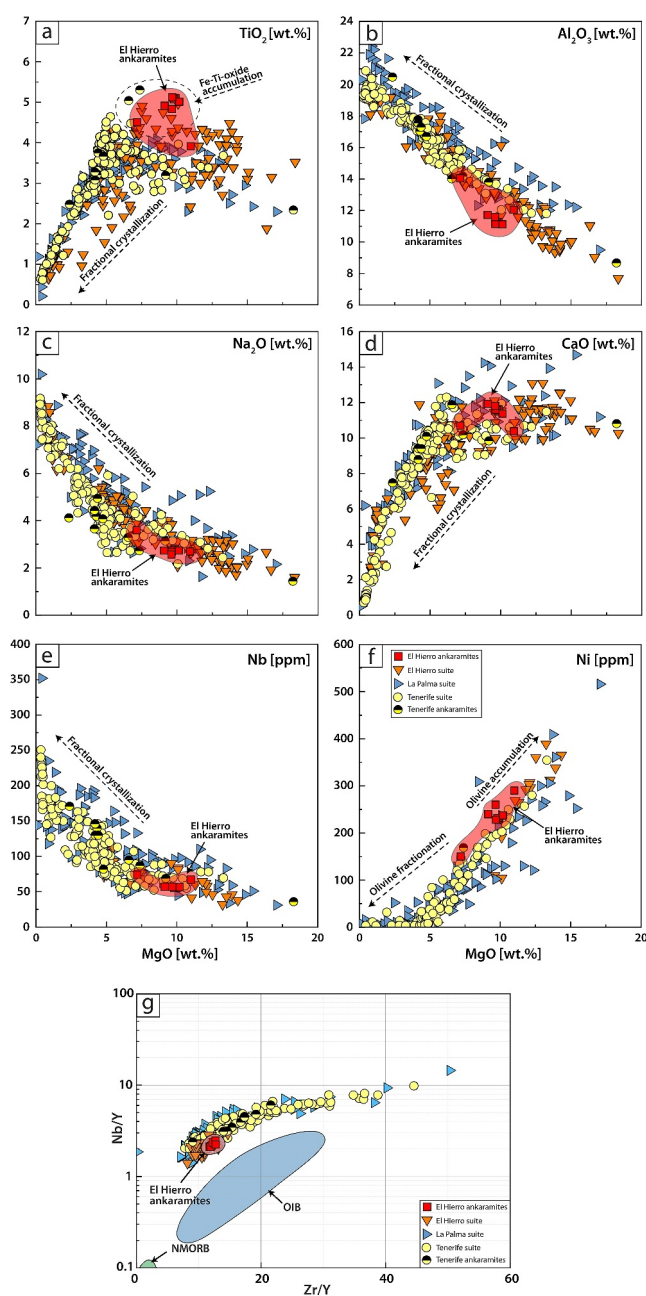
Figure 4. (a–f) MgO variation diagrams for El Hierro post-collapse ankaramites as well as other representative volcanic rocks from El Hierro, La Palma, and Tenerife. The overall curved major and trace element trends indicate fractional crystallization as the dominant process controlling compositional variations for El Hierro, La Palma, and Tenerife volcanic rocks, while trace element data also indicate a degree of accumulation. Additional data from Abratis et al. (2002); Carracedo et al. (2001); Deegan et al. (2012); Klügel et al. (2011); Pellicer (1979); Schmincke (1982). (g) Nb/Y versus Zr/Y plot for El Hierro post-collapse ankaramites and other El Hierro, La Palma, and Tenerife volcanic rocks with reference fields for normal mid-ocean ridge basalt (NMORB) and OIB (after Fitton et al., 1997, 2003). El Hierro ankaramites and most other Canary Island volcanic rocks plot outside the reference field for NMORB and OIB because they are results of fractionation and accumulation rather than being primary melts. Additional data from Abratis et al. (2002); Carracedo et al. (2001); Deegan et al. (2012); Klügel et al. (2011); Schmincke (1982).

bombs, we derived parental magma water contents between 0.24 ± 0.07 and 3.20 ± 0.64 wt.% (Figure 6; see Supporting Information S1 for full data set). This wide range of water contents implies the contribution of magma batches from different reservoirs and intrusions and/or sampling of such reservoirs over time.
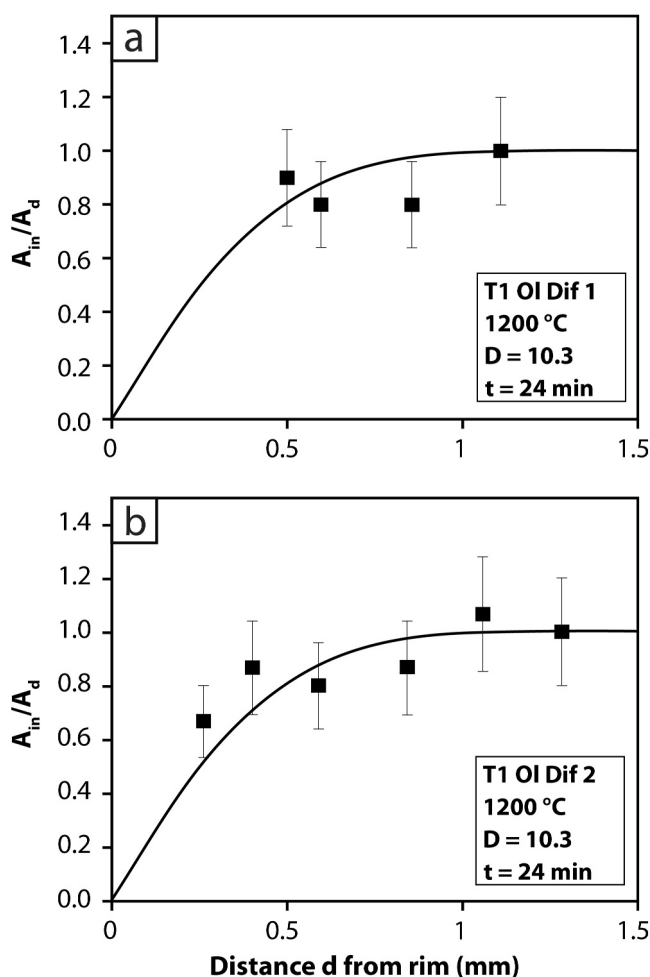
Figure 5. Diffusion profiles for hydrogen in two olivine crystals from sample T1. (a) Profile for crystal T1 ol Dif1. No clear diffusion profile can be seen from the core to the rim; however, considering the error in water content, a rough fit for the diffusion curve was achieved when applying olivine diffusion data for cation diffusion at 1200°C ($\log_D = -10.4$). (b) Diffusion profile for crystal T1 ol Dif2. Here, a clearer profile from core to rim is observed. For both crystals the best fit for the curve was achieved for a diffusion time interval of about 30 min.

To calculate parental magmatic water content on the basis of olivine, we used mineral compositional data in tandem with the partition coefficient determined by Le Voyer et al. (2014). This approach is based on a direct comparison between olivine compositions and their host magma as recorded by melt inclusions found in the crystals. Calculated magmatic volatile contents for olivine from lava bomb samples range from 0.29 ± 0.09 to 2.43 ± 0.78 wt.% and the maximum is hence much lower than maximum water contents determined through clinopyroxene (Figure 7). Magmatic water contents determined through olivine are, however, similar to the established range in ocean island basalts globally (~1 wt.% H_2O; Deegan et al., 2012; Dixon et al., 1997; Dixon & Clague, 2001; Gurenko & Schmincke, 2000; Kovalenko et al., 2007; Moore, 1970; Sides et al., 2014; Simons et al., 2002; Wallace, 1998a, b; Weis et al., 2015).

The analyzed melt inclusions record water contents between 0.20 ± 0.04 and 1.1 ± 0.2 wt.% H_2O, which overlap with the values determined from hydrogen defects in olivine crystals and thus confirm relatively low water content during olivine crystallization (Figure 6). Some of the melt inclusions in olivine showed evidence for partial crystallization and the determined water contents may thus be viewed as a maximum estimate for magmatic water in melt inclusions, as re-homogenization of partially crystallized inclusions would lead to lower H_2O contents (e.g., Ni et al., 2017).
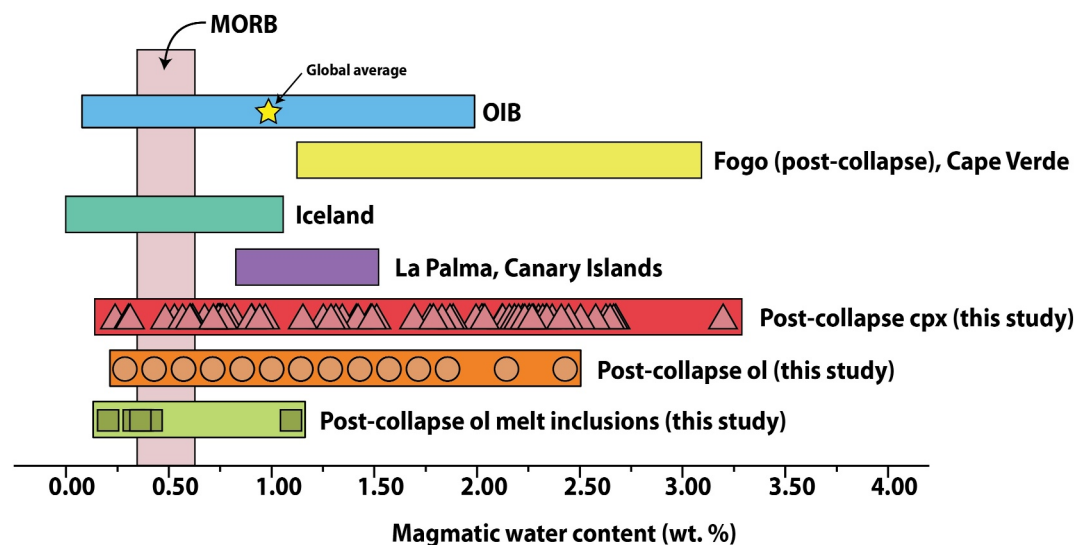
Figure 6. Comparison of magmatic water contents of El Hierro post El Golfo collapse eruptives, post-collapse Fogo eruptives (Cape Verde), La Palma (Canary Islands), Iceland, and other Ocean Island Basalt (OIB) and Mid-Ocean Ridge Basalt (MORB) compositions. Standard MORB (UOB reference material) values are from Bindeman et al. (2022); water values for OIBs are from Deegan et al. (2012); Dixon et al. (1997); Dixon and Clague (2001); Gurenko and Schmincke (2000); Kovalenko et al. (2007); Moore (1970); Sides et al. (2014); Wallace (1998a, 1998b); Weis et al. (2015). Values for Fogo are from DeVitre et al. (2023) and Lo Forte et al. (2023), for La Palma from Weis et al. (2015), and Iceland from Radu et al. (2023).
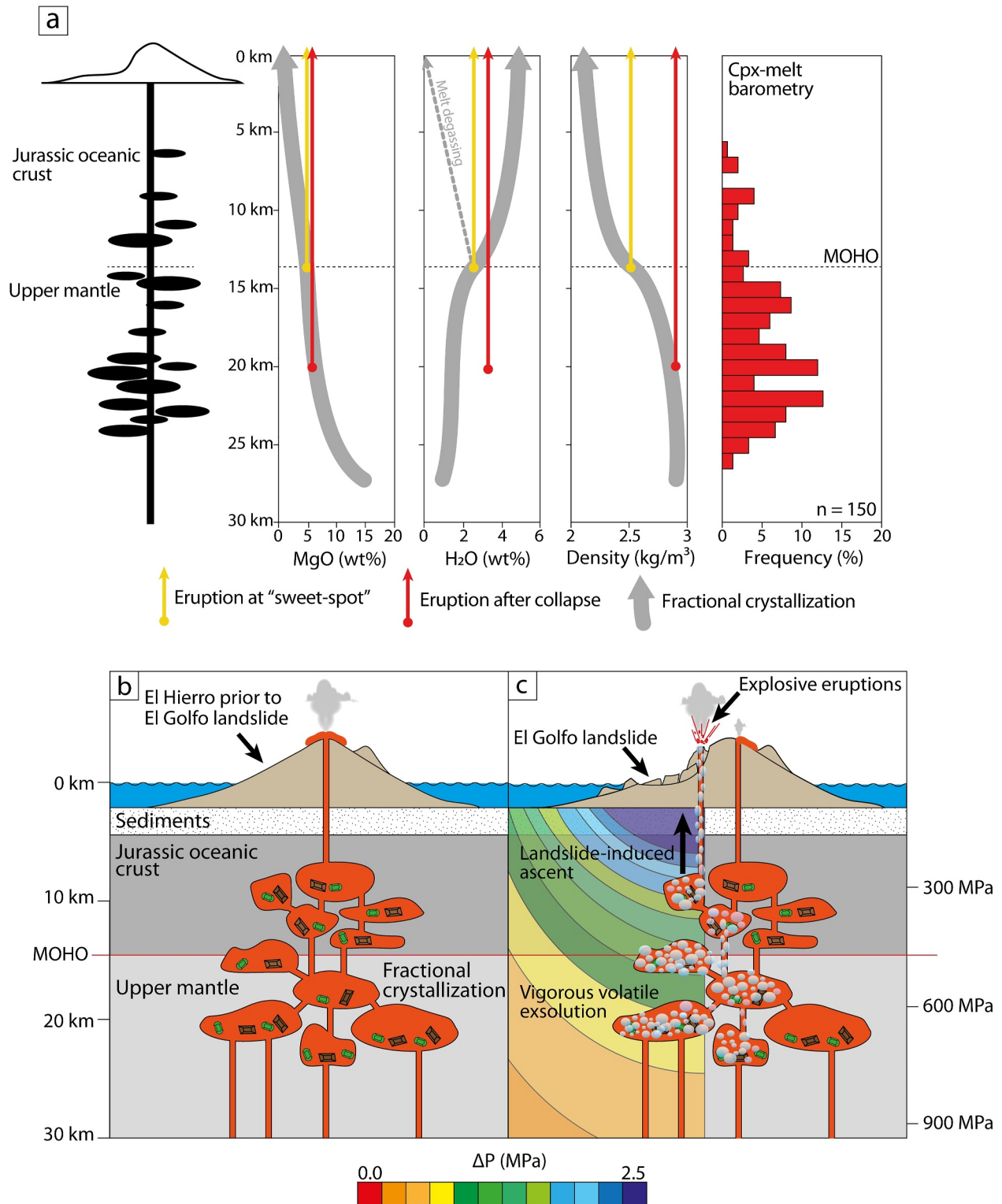
4.5. Clinopyroxene-Melt Thermobarometry

Testing for equilibrium between clinopyroxene crystals extracted from the volcanic bomb and ankaramite lava samples and possible melts revealed that out of 179 tested analytical points from 39 clinopyroxene crystals, 150 are in equilibrium with a melt represented by the averaged groundmass data (see Supporting Information S1 for full equilibrium test calculations). While crystals in equilibrium with the groundmass represent the last pre-eruptive storage conditions, whole rock represents an earlier liquid and hence, an earlier stage of magma evolution. Using the thermobarometry models of Putirka (2008, Eq. 33) and Neave and Putirka (2017) that are calibrated for ultramafic to intermediate compositions with a magmatic water content of 3 wt.% (see magmatic water calculation section) results in crystallization temperatures and pressures of 1099–1223°C and 155–755 MPa, respectively. These crystallization pressures correspond to depths between 5 and 26 km with the majority of the data clustering around 20–23 km depth and are therefore mostly below the crust-mantle boundary, which is located at ~14–15 km depth beneath El Hierro (e.g., Ranero et al., 1995). This realization points to magma storage in the lower crust to upper mantle below the island, specifically in the region considered as the underplating zone beneath the Canary Islands with a very small proportion of shallow grown crystals (cf. Carracedo, Troll, et al., 2015; Hansteen et al., 1998; Klügel et al., 2005, 2015; Marti et al., 2013; Ubide et al., 2022).

5. Discussion

5.1. Magmatic Water Contents in OIBs

Since the investigated rock samples are dominantly derived from pyroclastic deposits, syn- or post-eruptive dehydration through redox-processes was most likely minor (cf. Wade et al., 2008). However, the very low water contents in clinopyroxene from two lava bomb samples indicate potential dehydration of the majority of their crystals ($n = 24$). This would be consistent with rehydration experiments on a small number ($n = 10$) of Tanganasoga clinopyroxene (Weis et al., 2016) that point to dehydration of these crystals as a consequence of oxidation and minor magmatic degassing before eruption (cf. Longpré et al., 2017). In addition, clinopyroxene from the sampled lava flows exhibited the lowest water content in this study (18–114 ppm H_2O), which is not surprising considering that extensive volatile loss and crystal dehydration have previously been described for crystals in effusive lava samples (cf. Lloyd et al., 2016; Weis et al., 2015). The rehydration experiments of Weis et al. (2016) indicate that clinopyroxene water contents ≥600 ppm may be near or equal to pristine magmatic

Figure 7. (a) Thermobarometry reveals that clinopyroxene of this study grew between 5 and 26 km depth with a crystallization peak at 20–23 km, implying that hydrogen incorporation into clinopyroxene structural defects dominantly occurred in the upper mantle and up to ~11 km below the Moho beneath El Hierro. The dense and crystal-rich ankaramite magmas are usually hampered in their ascent due to the load of the volcanic edifice (e.g., Carracedo, Pérez-Torrado, et al., 2015; Pinel & Jaupart, 2000, 2004) and thus underplate the island. Vertical unloading can cause a pressure change at depth (Manconi et al., 2009) at delayed time scales of up to 50 ka (Cornu et al., 2021) and allows crystal- and H_2O-rich ankaramite magmas to rapidly ascend and erupt explosively within and around the landslide embayment. Comparison of the "eruptible sweet-spot" (modified after Ubide et al., 2022) with our data for El Hierro shows that post-collapse volcanism of the El Golfo embayment

water contents in post-collapse clinopyroxene, whereas crystals below this value reflect hydrogen loss. Consequently, only clinopyroxene crystals with water contents above this value ($n = 30$) are considered to be reflective of original magmatic water contents.

The water contents derived from clinopyroxene crystals (up to 3.20 ± 0.64 wt.%) in this study overlap with previous H_2O values obtained from experimentally rehydrated clinopyroxene crystals from the same ankaramite samples (up to 3.88 ± 0.78 wt.%; see Weis et al., 2016), implying that the highest recorded values in this study are a reliable reflection of the magmatic H_2O content of post-collapse magmas erupted within the El Golfo embayment on El Hierro. Employing the volatile approximation method of Dixon et al. (1997; H_2O wt. % $\approx 3 \times [P_2O_5]$) as an independent test of the water contents in our samples results in values of up to 2.0 ± 0.1 wt. % H_2O. Although the method of Dixon et al. (1997) provides only a rough, and likely minimum water estimate, the results overlap with the lower end of our non-dehydrated clinopyroxene-derived values, and thus corroborate the high water contents measured in the post-collapse ankaramite magmas.

Our new H_2O results from post El Golfo collapse clinopyroxene also compare well with water contents measured in olivine-hosted melt inclusions from the basanite magmas of the submarine 2011–2012 El Hierro eruption (0.4– 3.0 wt.% H_2O; Longpré et al., 2017) as well as with data for melt inclusions in young (<20 ka; 0.06–2.22 wt.% H_2O) basanites from El Hierro presented in Taracsák et al. (2019). The high H_2O contents we obtained from clinopyroxene are further consistent with H_2O values determined from ankaramites from the post-collapse pyroclastic deposits and lava of the Teno massif on Tenerife (0.75–2.22 wt.% H_2O; Longpré et al., 2009). Teno is a Miocene to Pliocene shield volcano that, like El Hierro, experienced several giant landslides at ~4.1 Ma, followed by extensive post-collapse ankaramite volcanism with highly explosive episodes (Longpré et al., 2008, 2009; Walter et al., 2005). Additionally, our results also support recent findings of high OIB magmatic water contents on other ocean islands beyond the Canary archipelago, which have not undergone flank collapse or other load-removal events. Notably, high magmatic H_2O contents derived from clinopyroxene in basalts from the Cook-Austral Islands, French Polynesia (0.35–4.25 wt.% H_2O; Bruce-Etzel et al., 2024) and clinopyroxene in basalts to basaltic trachyandesites from Bermuda (1.9–5.7 wt% H_2O; Mazza et al., 2019), along with our results of up to 3.20 ± 0.64 wt.% H_2O suggest that previous estimates of magmatic water content in ocean island magmas may have been underestimated.

Our results therefore contrast the established view that OIB magmas are relatively water poor, as OIB-type basalts, basanites, and ankaramites usually range from 0.08 to 1.95 wt.% H_2O, with an average of ~1.0 wt.% H_2O (Figure 6; Deegan et al., 2012; Dixon & Clague, 2001; Dixon et al., 1997; Gurenko & Schmincke, 2000; Kovalenko et al., 2007; Moore, 1970; Sides et al., 2014; Wallace, 1998a, 1998b; Weis et al., 2015) and add to a growing body of evidence that some OIB magmas may be considerably more water rich than widely assumed.

5.2. A Model for Water Enrichment in OIB Underplating Zones

Water contents derived from olivine crystals (0.29 ± 0.04 to 2.43 ± 0.78 wt.%) from the ankaramite bombs are, with few exceptions, lower than the values derived from clinopyroxene and average around 1 wt.% H_2O, which is close to the global OIB average. The distribution of water contents in olivine crystals from the ankaramite bomb samples is relatively homogeneous compared to clinopyroxene, which may be a consequence of distinct dehydration mechanisms for olivine relative to clinopyroxene. This is because cation and vacancy diffusion, which is the dominant dehydration mechanism in olivine, is slower than hydrogen diffusion and associated hydrogen loss by redox processes in Fe-rich clinopyroxene ($\log_D = -10$ vs. -11 at ~1100°C; Demouchy & Mackwell, 2006; Hercule & Ingrin, 1999). This is also supported by the absence of hydrogen diffusion profiles in olivine crystals. Thus, if a sudden drop in volatile pressure led to rapid hydrogen loss in some clinopyroxene crystals via redox-processes prior to quenching (cf. Weis et al., 2016), the slower vacancy diffusion in olivine crystals should have led to slower hydrogen loss. Hence, the water contents in olivine from ankaramite bombs (0.29 ± 0.04 to 2.43 ± 0.78 wt.%, average 0.88 ± 0.28 wt.%) more probably represent magmatic H_2O contents at the time of

has higher contents of MgO and H_2O as well as a higher magmatic density than the proposed sweet-spot. We thus argue that unloading effects after the El Golfo landslide triggered the ascent of these otherwise difficult to erupt magmas. (b and c) Simplified sketch of the magma plumbing system underneath El Hierro based on concepts in Carracedo, Troll, et al. (2015); Gonzalez et al. (2013); Manconi et al. (2009); Oglialoro et al. (2017); Stroncik et al. (2009) and on our new results. The colored pressure scale shows the effect on pressure in the upper mantle caused by the El Golfo landslide. According to the model by Manconi et al. (2009), the landslide caused a drop in pressure in the main magma storage levels (20–23 km depth) of ~0.5–0.6 MPa, causing a decompression within the magma plumbing dynamics.

olivine crystallization. If correct, this implies that olivine records an initial water content of the melts that is more consistent with "normal" OIB melts. The low magmatic water contents derived from olivine crystals are also supported by the values derived from the olivine-hosted melt inclusions (0.20 ± 0.04 to 1.1 ± 0.2 wt.% H_2O) and both support a low water content in the initial melt. This, however, contrasts melt inclusions found in olivine from the post-collapse eruptives of the Fogo system in the Cape Verde Islands, which record higher water contents of up to 2.92 wt% H_2O and that have been entrapped at around ∼31 km depth, that is, within the upper mantle below Fogo (DeVitre et al., 2023; Lo Forte et al., 2023). A major volcano flank collapse occurred at ∼68 ka at Fogo and is thought to have had unloading effects up to a depth of 30 km below the island. Hence, eruption of water-rich magmas stored at this depth may also be facilitated by rapid unloading in ocean islands and could be similar to the scenario for post-collapse volcanism in the El Golfo embayment. The concept of "wet" OIB magmas evolving and being stored in underplating zones thus likely applies also to other ocean islands with underplating zones.

The relatively low H_2O values in olivine and their low calculated magmatic H_2O contents compared to the higher magmatic water contents derived through clinopyroxene have implications for magma evolution below El Hierro. The observed discrepancy between olivine and clinopyroxene implies that extensive crystallization of OIB magmas in underplating zones (at up to 26 km depth according to our thermobarometry results) leads to progressively elevated volatile contents at upper mantle levels, that is, during the main clinopyroxene crystallization stage in these samples. This can be the case when primitive mantle melts migrate from the upper mantle into the underplating zone near the Moho, where they begin to crystallize and fractionate (cf. Carracedo, Troll, et al., 2015; Hansteen et al., 1998; Klügel et al., 2015; Manconi et al., 2009). We argue that these magmas are initially water-poor, as indicated by our olivine data and data from Teno ankaramites (Longpré et al., 2009), but fractional crystallization of up to possibly several % in the underplating zone (e.g., Carracedo, Troll, et al., 2015; Hansteen et al., 1998; Klügel et al., 2015; Manconi et al., 2009) then results in enrichment of dissolved volatiles in the melt.

To further test if volatile enrichment is caused by crystallization and crystal fractionation, equilibrium between the phenocrysts and their host melt can be tested by calculating the corresponding

$$K_{D\,crystal-melt}^{Fe-Mg} \left(= \frac{\frac{X_{melt}^{MgO}}{X_{crystal}^{MgO}}}{\frac{X_{melt}^{FeO}}{X_{crystal}^{FeO}}} \right).$$

For clinopyroxene, equilibrium can be assumed if K_D ranges from 0.20 to 0.36 (see Putirka, 2008), while olivine should return values between 0.27 and 0.35 (cf. Matzen et al., 2011; Roeder & Emslie, 1970). Clinopyroxene crystals show K_D values between 0.29 and 0.30 and are thus in equilibrium with the whole rock composition of our samples. Post El Golfo collapse olivine crystals ($n = 61$) show K_D values between 0.37 and 0.51, with the majority above 0.41, and are neither in equilibrium with their host rock compositions nor with groundmass (melt) compositions, implying they grew in an earlier stage of evolution from a less evolved (more primitive) melt or magma. The lower range of magmatic H_2O reported from olivine crystals together with most clinopyroxene crystals being in equilibrium with their whole rock compositions, but not with their groundmass, implies continuous melt evolution. This also implies that olivine crystallization would have preceded pyroxene crystallization in the post-collapse magmas. Therefore, the parental magmas crystallizing olivine did not have unusually high initial magmatic water contents, which supports the concept of initially dry OIB melts that subsequently become enriched in volatiles during fractional crystallization.

Fractionation of post-collapse eruptives is also supported by trace element ratios such as Nb/Y versus Zr/Y. Our ankaramites, along with most other Canary Island rocks from the literature, do not overlap with the established reference fields for NMORB and OIB (Figure 4g; after Fitton et al., 1997, 2003). Instead, ankaramites as well as most other El Hierro, La Palma and Tenerife volcanic rocks plot at distinctly higher Nb/Y and Zr/Y ratios and hence do not represent a primary mantle melt but rather a fractionated, water-enriched magma.

5.3. Magma Plumbing, Storage and Eruptibility Under Ocean Islands

It was recently proposed that plumbing systems underneath ocean islands act as geochemical filters for ascending magmas (cf. Klügel et al., 2015; Ubide et al., 2022). Ubide et al. (2022) suggested that on El Hierro, as well as on

other ocean islands, near-primary melts do not generally erupt. Instead, primary melts that pass through volcanic plumbing systems fractionate en route to the surface, and eventually reach basaltic compositions with ca. 5 wt.% MgO, which have density and volatile concentrations that can facilitate an eruption (Ubide et al., 2022). However, OIB whole-rock analyses usually return MgO contents of more than 10 wt.%, pointing to obfuscation of the more evolved melt signal by the pheno- and antecryst cargo of the melt. Crystal-free whole rocks, glasses and melt-inclusions, in turn, usually return compositions around the expected 5 wt.% MgO, pointing to an "eruptible sweet-spot" at which volatile saturation along with eruptible density and viscosity values are reached (Ubide et al., 2022). These magmas commonly erupt in non-explosive fashion, resulting in lava flows at the surface and associated feeder dykes at depth. Our samples show average MgO values of 9.84 wt.% for whole rock analyses, while phenocryst-free matrix analyses record average MgO values of 5.85 wt.%. While our samples hence overlap with the "eruptible sweet-spot" in terms of MgO content, the magmatic water content calculated for our samples (3.2 ± 0.64 wt.%; Figure 7a) exceeds the proposed ≤2.5 wt.% volatile content threshold. In addition, ankaramite melts have a density of ~2.95 kg/m^3 (Manconi et al., 2009), which is well above the suggested ~2.50 kg/m^3, that is, lying above the "eruptible sweet-spot" (Figure 7a; Ubide et al., 2022). We thus argue that while our samples are close to the "eruptible sweet-spot" in terms of their chemical composition, they may be too dense to erupt solely by themselves and we hypothesize that unloading was an additional trigger facilitating eruption of the high-density ankaramites analyzed in this study. The higher volatile content observed in our samples would then facilitate rapid ascent and may explain the in part explosive eruptive behavior during post-collapse volcanism on El Hierro. This is indirectly supported by high ascent rates. While ascent rate estimates for effusive, vesicular basanite lava on La Palma are around 0.2 m/s (Klügel et al., 1997), using the diffusion profile observed in one of our olivine crystals resulted in extremely fast ascent rates between 23 and 31 m/s (see additional discussion in Supporting Information S1), which would be in line with rapid ascent triggered by a major event, such as a large vertical unloading event.

We observed that while some post-collapse clinopyroxene lost a portion of their primary water content, the majority remained saturated, implying that the parental magma had relatively high H_2O contents prior to eruption when compared with average OIB magma compositions. Although mafic in character, we have shown that the investigated samples are not primary melts. Mafic Canary magmas are initially stored in upper mantle under-plating reservoirs between 15 and 30 km depth where they undergo extensive low-pressure fractionation and degassing during polybaric ascent (Hansteen et al., 1998; Klügel et al., 2000, 2005; Longpré et al., 2017; Stroncik et al., 2009). Our thermobarometry results reveal a clinopyroxene crystallization peak at ~20 km depth, which overlaps with the depth range assumed for the underplating zone beneath the Canary Islands (Carracedo, Troll, et al., 2015; Hansteen et al., 1998; Klügel et al., 2015; Manconi et al., 2009). Stored at this depth, dense but volatile rich magmas usually do not erupt since the load of a volcanic edifice may act as a density filter on a volcano's plumbing system, commonly preventing dense mafic and progressively crystal-rich magmas from ascending (Cassidy et al., 2015; Pinel & Jaupart, 2000, 2004). Removing parts of the edifice load during, for example, glacial melting or giant landslide events will cause a decompression effect that translates through the crust into the upper mantle (down to ≥40 km) and can thus temporarily shift the density limit for ascending magmas (e.g., Cassidy et al., 2015; Hooper et al., 2011; Manconi et al., 2009; Pinel & Jaupart, 2000, 2004; Spaans et al., 2015). Magma that resides at depth but is close to the critical window of eruptibility due a high crystal-, but also high volatile content from fractional crystallization (i.e., close to the critical gas content-viscosity-density window) can then ascend with considerable speed and erupt as a result of crustal unloading. This would also explain the sometimes explosive nature of the post-El Golfo collapse eruptions and similar young vents within recent and large landslide scars on the Canary Islands, such as at Teno on Tenerife. The resulting pressure change induced by the El Golfo giant collapse is estimated to range between 0.7 and 0.8 MPa at ~20 km depth (Manconi et al., 2009), which likely led to gas exsolution in water rich magmas of the underplating zone and consequently to temporary reduction of magma density (cf. Cashman, 2004; Gardner et al., 1999). This process could then promote the sudden ascent of the water-rich ankaramite magma (Figures 7b and 7c).

6. Conclusions

Through our investigation, we have shown that magmatic water contents of mafic upper mantle magmas from the underplating zone underneath El Hierro can considerably exceed the average H_2O content of usual OIB-type basaltic magmas. Our results are in agreement with models of fast magma ascent triggered by magma fractionation in underplating zones coupled with effects of vertical unloading that can cause dense and crystal rich

magmas to ascent due to high volatile content and may even result in at times explosive eruptive behavior, as recorded at for example, Tanganasoga and other post-collapse vents within the El Golfo embayment. Importantly, while OIB magmas may be generally volatile-poor due to low source volatile concentrations and volatile loss during polybaric ascent, volatile-rich magmas may temporarily exist during upper mantle storage. Such mafic but volatile-rich magmas would usually remain hidden due to their high density and the high overload pressure and therefore become part of the extensive plutonic suites added to the base of the island during ongoing magmatic underplating.

We therefore argue that the combination of the upper mantle magma underplating zone and mantle decompression that promotes post-collapse volcanism enables dense but volatile rich magmas to erupt during and after episodes of rapid vertical unloading. Thus, our results offer a unique glimpse into the compositional spectrum, volatile content, and magmatic processes at play in sub-ocean island underplating zones.

Data Availability Statement

The original data presented in this study are available in the Data Set S1 in Excel format. Figures 3a, 4, and 6 contain a compilation of geochemical data for El Hierro, La Palma, and Tenerife used in this study for comparative purposes and are available in the respective cited publications and their Supporting Information. Figure 7a was, in part, redrawn after Ubide et al. (2022); the original figure and the data it is based on can be found in the cited publication. The obtained FTIR spectra were processed with PeakFit, a commercial peak separation and analysis software by SigmaPlot. Thermobarometry modeling was conducted with the "Clinopyroxene P-T" Excel spreadsheet freely available on Keith Putirka's personal website (https://csm.fresnostate.edu/ees/faculty-staff/putirka.html).

References

Abratis, M., Schmincke, H. U., & Hansteen, T. (2002). Composition and evolution of submarine volcanic rocks from the central and western Canary Islands. *International Journal of Earth Sciences*, *91*(4), 562–582. https://doi.org/10.1007/s00531-002-0286-7

Amelung, F., & Day, S. (2002). InSAR observations of the 1995 Fogo, Cape Verde, eruption: Implications for the effects of collapse events upon island volcanoes. *Geophysical Research Letters*, *29*(12), 47-1-47-4. https://doi.org/10.1029/2001GL013760

Barker, A. K., Troll, V. R., Carracedo, J. C., & Nicholls, P. A. (2015). The magma plumbing system for the 1971 Teneguía eruption on La Palma, Canary Islands. *Contributions to Mineralogy and Petrology*, *170*(5–6), 54. https://doi.org/10.1007/s00410-015-1207-7

Beran, A. (1976). Messung des Ultrarot-Pleochroismus von Mineralen. XIV. Der Pleochroismus der OH-Streckfrequenz in Diopsid. *Tschermaks Mineralogische und Petrographische Mitteilungen*, *23*(2), 79–85. https://doi.org/10.1007/BF01081476

Bindeman, I. N., Deegan, F. M., Troll, V. R., Thordarson, T., Höskuldsson, Á., Moreland, W. M., et al. (2022). Diverse mantle components with invariant oxygen isotopes in the 2021 Fagradalsfjall eruption, Iceland. *Nature Communications*, *13*(1), 3737. https://doi.org/10.1038/s41467-022-31348-7

Brey, G., & Schmincke, H. U. (1980). Origin and diagenesis of the Roque Nublo breccia, Gran Canaria (Canary Islands) — Petrology of Roque Nublo Volcanics, II. *Bulletin Volcanologique*, *43*(1), 15–33. https://doi.org/10.1007/BF02597608

Brown, G. E. (1980). Olivines and silicate spinels. *Reviews in Mineralogy and Geochemistry*, *5*(1), 275–381.

Bruce-Etzel, L. A., Marshall, E. W., & Lassiter, J. C. (2024). Magmatic water content in HIMU basalts from the Cook-Austral Islands: Constraints on degassing processes and source composition from clinopyroxene phenocrysts. *Contributions to Mineralogy and Petrology*, *179*(83), 83. https://doi.org/10.1007/s00410-024-02160-x

Carracedo, J. C. (1994). The Canary Islands: An example of structural control on the growth of large oceanic-island volcanoes. *Journal of Volcanology and Geothermal Research*, *60*(3–4), 225–241. https://doi.org/10.1016/0377-0273(94)90053-1

Carracedo, J. C. (1999). Growth, structure, instability and collapse of Canarian volcanoes and comparisons with Hawaiian volcanoes. *Journal of Volcanology and Geothermal Research*, *94*(1–4), 1–19. https://doi.org/10.1016/S0377-0273(99)00095-5

Carracedo, J. C., Guillou, H., Nomade, S., Rodriguez-Badiola, E., Perez-Torrado, F. J., Rodriguez-Gonzalez, A., et al. (2011). Evolution of ocean-island rifts: The northeast rift zone of Tenerife, Canary Islands. *Geological Society of America Bulletin*, *123*(3–4), 562–584. https://doi.org/10.1130/B30119.1

Carracedo, J. C., Pérez-Torrado, F. J., Rodríguez-González, A., Paris, R., Troll, V. R., & Barker, A. K. (2015). Volcanic and structural evolution of Pico do Fogo, Cape Verde. *Geology Today*, *31*(4), 146–152. https://doi.org/10.1111/gto.12101

Carracedo, J. C., Pérez-Torrado, F. J., Rodríguez-González, A., Soler, V., Fernández-Turiel, J. L., Troll, V. R., & Wiesmaier, S. (2012). The 2011 submarine volcanic eruption in El Hierro (Canary Islands). *Geology Today*, *28*(2), 53–58. https://doi.org/10.1111/j.1365-2451.2012.00827.x

Carracedo, J. C., Rodríguez-Badiola, E., Guillou, H., De La Nuez, J., & Pérez-Torrado, F. J. (2001). Geología y vulcanología de La Palma y El Hierro, Canarias Occidentales. *Estudios Geológicos*, *57*(5–6), 175–273. https://doi.org/10.3989/egeol.01575-6134

Carracedo, J. C. & Troll, V. R. (Eds.) (2013)., *Teide volcano: Geology and eruptions of a highly differentiated oceanic stratovolcano*. Springer Berlin Heidelberg. https://doi.org/10.1007/978-3-642-25893-0

Carracedo, J. C., & Troll, V. R. (2016). *The geology of the Canary Islands*. Elsevier.

Carracedo, J. C., Troll, V. R., Day, J. M. D., Geiger, H., Aulinas, M., Soler, V., et al. (2022). The 2021 eruption of the Cumbre Vieja volcanic ridge on La Palma, Canary Islands. *Geology Today*, *38*(3), 94–107. https://doi.org/10.1111/gto.12388

Carracedo, J. C., Troll, V. R., Zaczek, K., Rodríguez-González, A., Soler, V., & Deegan, F. M. (2015). The 2011–2012 submarine eruption off El Hierro, Canary Islands: New lessons in oceanic island growth and volcanic crisis management. *Earth-Science Reviews*, *150*, 168–200. https://doi.org/10.1016/j.earscirev.2015.06.007

Cashman, K. V. (2004). Volatile controls on magma ascent and eruption. In R. S. J. Sparks & C. J. Hawkesworth (Eds.), *Geophysical Monograph Series* (Vol. 150, pp. 109–124). American Geophysical Union. https://doi.org/10.1029/150GM10

Cassidy, M., Watt, S. F. L., Talling, P. J., Palmer, M. R., Edmonds, M., Jutzeler, M., et al. (2015). Rapid onset of mafic magmatism facilitated by volcanic edifice collapse. *Geophysical Research Letters*, *42*(12), 4778–4785. https://doi.org/10.1002/2015GL064519

Cornu, M. N., Paris, R., Doucelance, R., Bachélery, P., Bosq, C., Auclair, D., et al. (2021). Exploring the links between volcano flank collapse and the magmatic evolution of an ocean island volcano: Fogo, Cape Verde. *Scientific Reports*, *11*(1), 17478. https://doi.org/10.1038/s41598-021-96897-1

Day, S. J., Carracedo, J. C., & Guillou, H. (1997). Age and geometry of an aborted rift flank collapse: The San Andres fault system, El Hierro, Canary Islands. *Geological Magazine*, *134*(4), 523–537. https://doi.org/10.1017/S0016756897007243

Deegan, F. M., Troll, V. R., Barker, A. K., Harris, C., Chadwick, J. P., Carracedo, J. C., & Delcamp, A. (2012). Crustal versus source processes recorded in dykes from the Northeast volcanic rift zone of Tenerife, Canary Islands. *Chemical Geology*, *334*, 324–344. https://doi.org/10.1016/j.chemgeo.2012.10.013

Demouchy, S., & Mackwell, S. (2003). Water diffusion in synthetic iron-free forsterite. *Physics and Chemistry of Minerals*, *30*(8), 486–494. https://doi.org/10.1007/s00269-003-0342-2

Demouchy, S., & Mackwell, S. (2006). Mechanisms of hydrogen incorporation and diffusion in iron-bearing olivine. *Physics and Chemistry of Minerals*, *33*(5), 347–355. https://doi.org/10.1007/s00269-006-0081-2

DeVitre, C. L., Gazel, E., Ramalho, R. S., Venugopal, S., Steele-MacInnis, M., Hua, J., et al. (2023). Oceanic intraplate explosive eruptions fed directly from the mantle. *Proceedings of the National Academy of Sciences*, *120*(33). https://doi.org/10.1073/pnas.2302093120

Dingwell, D. B. (1996). Volcanic dilemma—Flow or blow? *Science*, *273*(5278), 1054–1055. https://doi.org/10.1126/science.273.5278.1054

Dixon, J. E., & Clague, D. A. (2001). Volatiles in basaltic glasses from Loihi Seamount, Hawaii: Evidence for a relatively dry plume component. *Journal of Petrology*, *42*(3), 627–654. https://doi.org/10.1093/petrology/42.3.627

Dixon, J. E., Clague, D. A., Wallace, P., & Poreda, R. (1997). Volatiles in Alkalic basalts form the North Arch volcanic field, Hawaii: Extensive degassing of deep submarine-erupted Alkalic series lavas. *Journal of Petrology*, *38*(7), 911–939. https://doi.org/10.1093/petroj/38.7.911

Fitton, J. G., Saunders, A. D., Kempton, P. D., & Hardarson, B. S. (2003). Does depleted mantle form an intrinsic part of the Iceland plume? *Geochemistry, Geophysics, Geosystems*, *4*(3). https://doi.org/10.1029/2002GC000424

Fitton, J. G., Saunders, A. D., Norry, M. J., Hardarson, B. S., & Taylor, R. N. (1997). Thermal and chemical structure of the Iceland plume. *Earth and Planetary Science Letters*, *153*(3–4), 197–208. https://doi.org/10.1016/S0012-821X(97)00170-2

Gardner, J. E., Hilton, M., & Carroll, M. R. (1999). Experimental constraints on degassing of magma: Isothermal bubble growth during continuous decompression from high pressure. *Earth and Planetary Science Letters*, *168*(1–2), 201–218. https://doi.org/10.1016/S0012-821X(99)00051-5

Gee, M. J. R., Watts, A. B., Masson, D. G., & Mitchell, N. C. (2001). Landslides and the evolution of El Hierro in the Canary Islands. *Marine Geology*, *177*(3–4), 271–293. https://doi.org/10.1016/S0025-3227(01)00153-0

Geiger, H., Barker, A. K., & Troll, V. R. (2016). Locating the depth of magma supply for volcanic eruptions, insights from Mt. Cameroon. *Scientific Reports*, *6*(1), 33629. https://doi.org/10.1038/srep33629

González, P. J., Samsonov, S. V., Pepe, S., Tiampo, K. F., Tizzani, P., Casu, F., et al. (2013). Magma storage and migration associated with the 2011–2012 El Hierro eruption: Implications for crustal magmatic systems at oceanic island volcanoes. *Journal of Geophysical Research: Solid Earth*, *118*(8), 4361–4377. https://doi.org/10.1002/jgrb.50289

GRAFCAN. (2024). Cartográfica de Canarias. Retrieved from https://www.grafcan.es/

Guillou, H., Carracedo, J. C., Pérez-Torrado, F. J., & Rodríguez-Badiola, E. (1996). K-Ar ages and magnetic stratigraphy of a hotspot-induced, fast grown oceanic island: El Hierro, Canary Islands. *Journal of Volcanology and Geothermal Research*, *73*(1–2), 141–155. https://doi.org/10.1016/0377-0273(96)00021-2

Gurenko, A. A., & Schmincke, H. U. (2000). S concentrations and its speciation in Miocene basaltic magmas north and south of Gran Canaria (Canary Islands): Constraints from glass inclusions in olivine and clinopyroxene. *Geochimica et Cosmochimica Acta*, *64*(13), 2321–2337. https://doi.org/10.1016/S0016-7037(00)00353-7

Hansteen, T. H., Klügel, A., & Schmincke, H. U. (1998). Multi-stage magma ascent beneath the Canary Islands: Evidence from fluid inclusions. *Contributions to Mineralogy and Petrology*, *132*(1), 48–64. https://doi.org/10.1007/s004100050404

Hercule, S., & Ingrin, J. (1999). Hydrogen in diopside; diffusion, kinetics of extraction-incorporation, and solubility. *American Mineralogist*, *84*(10), 1577–1587. https://doi.org/10.2138/am-1999-1011

Hernández Pacheco, A. (1982). Sobre una posible erupción en 1793 en la isla de El Hierro (Canarias). *Estudios Geológicos*, *38*(1–2), 15–26.

Hooper, A., Ófeigsson, B., Sigmundsson, F., Lund, B., Einarsson, P., Geirsson, H., & Sturkell, E. (2011). Increased capture of magma in the crust promoted by ice-cap retreat in Iceland. *Nature Geoscience*, *4*(11), 783–786. https://doi.org/10.1038/ngeo1269

Houghton, B. F., & Gonnermann, H. M. (2008). Basaltic explosive volcanism: Constraints from deposits and models. *Geochemistry*, *68*(2), 117–140. https://doi.org/10.1016/j.chemer.2008.04.002

Klügel, A., Hansteen, T. H., & Galipp, K. (2005). Magma storage and underplating beneath Cumbre Vieja volcano, La Palma (Canary Islands). *Earth and Planetary Science Letters*, *236*(1–2), 211–226. https://doi.org/10.1016/j.epsl.2005.04.006

Klügel, A., Hansteen, T. H., & Schmincke, H. U. (1997). Rates of magma ascent and depths of magma reservoirs beneath La Palma (Canary Islands). *Terra Nova*, *9*(3), 117–121. https://doi.org/10.1046/j.1365-3121.1997.d01-15.x

Klügel, A., Hansteen, T. H., van den Bogaard, P., Strauss, H., & Hauff, F. (2011). Holocene fluid venting at an extinct Cretaceous seamount, Canary archipelago. *Geology*, *39*(9), 855–858. https://doi.org/10.1130/G32006.1

Klügel, A., Hoernle, K. A., Schmincke, H. U., & White, J. D. L. (2000). The chemically zoned 1949 eruption on La Palma (Canary Islands): Petrologic evolution and magma supply dynamics of a rift zone eruption. *Journal of Geophysical Research*, *105*(B3), 5997–6016. https://doi.org/10.1029/1999JB900334

Klügel, A., Longpré, M. A., García-Cañada, L., & Stix, J. (2015). Deep intrusions, lateral magma transport and related uplift at ocean island volcanoes. *Earth and Planetary Science Letters*, *431*, 140–149. https://doi.org/10.1016/j.epsl.2015.09.031

Kovacs, I., Hermann, J., O'Neill, H. S. C., Gerald, J. F., Sambridge, M., & Horvath, G. (2008). Quantitative absorbance spectroscopy with unpolarized light: Part II. Experimental evaluation and development of a protocol for quantitative analysis of mineral IR spectra. *American Mineralogist*, *93*(5–6), 765–778. https://doi.org/10.2138/am.2008.2656

Kovalenko, V. I., Naumov, V. B., Girnis, A. V., Dorofeeva, V. A., & Yarmolyuk, V. V. (2007). Volatiles in basaltic magmas of ocean islands and their mantle sources: I. Melt compositions deduced from melt inclusions and glasses in the rocks. *Geochemistry International*, *45*(2), 105–122. https://doi.org/10.1134/S0016702907020012

Le Voyer, M., Asimow, P. D., Mosenfelder, J. L., Guan, Y., Wallace, P. J., Schiano, P., et al. (2014). Zonation of H_2O and F concentrations around melt inclusions in olivines. *Journal of Petrology*, *55*(4), 685–707. https://doi.org/10.1093/petrology/egu003

Libowitzky, E., & Rossman, G. R. (1996). Principles of quantitative absorbance measurements in anisotropic crystals. *Physics and Chemistry of Minerals*, *23*(6), 319–327. https://doi.org/10.1007/BF00199497

Libowitzky, E., & Rossman, G. R. (1997). An IR absorption calibration for water in minerals. *American Mineralogist*, *82*(11–12), 1111–1115. https://doi.org/10.2138/am-1997-11-1208

Lloyd, A. S., Ferriss, E., Ruprecht, P., Hauri, E. H., Jicha, B. R., & Plank, T. (2016). An assessment of clinopyroxene as a recorder of magmatic water and magma ascent rate. *Journal of Petrology*, *57*(10), 1865–1886. https://doi.org/10.1093/petrology/egw058

Lo Forte, F. M., Aiuppa, A., Rotolo, S. G., & Zanon, V. (2023). Temporal evolution of the Fogo Volcano magma storage system (Cape Verde Archipelago): A fluid inclusions perspective. *Journal of Volcanology and Geothermal Research*, *433*, 107730. https://doi.org/10.1016/j.jvolgeores.2022.107730

Longpré, M. A., Chadwick, J. P., Wijbrans, J., & Iping, R. (2011). Age of the El Golfo debris avalanche, El Hierro (Canary Islands): New constraints from laser and furnace 40Ar/39Ar dating. *Journal of Volcanology and Geothermal Research*, *203*(1–2), 76–80. https://doi.org/10.1016/j.jvolgeores.2011.04.002

Longpré, M. A., Stix, J., Klügel, A., & Shimizu, N. (2017). Mantle to surface degassing of carbon- and sulphur-rich alkaline magma at El Hierro, Canary Islands. *Earth and Planetary Science Letters*, *460*, 268–280. https://doi.org/10.1016/j.epsl.2016.11.043

Longpré, M. A., Troll, V. R., & Hansteen, T. H. (2008). Upper mantle magma storage and transport under a Canarian shield-volcano, Teno, Tenerife (Spain). *Journal of Geophysical Research*, *113*(B8). https://doi.org/10.1029/2007JB005422

Longpré, M. A., Troll, V. R., Walter, T. R., & Hansteen, T. H. (2009). Volcanic and geochemical evolution of the Teno massif, Tenerife, Canary Islands: Some repercussions of giant landslides on ocean island magmatism. *Geochemistry, Geophysics, Geosystems*, *10*(12). https://doi.org/10.1029/2009GC002892

Manconi, A., Longpré, M. A., Walter, T. R., Troll, V. R., & Hansteen, T. H. (2009). The effects of flank collapses on volcano plumbing systems. *Geology*, *37*(12), 1099–1102. https://doi.org/10.1130/G30104A.1

Martí, J., Castro, A., Rodriguez, C., Costa, F., Carrasquilla, S., Pedreira, R., & Bolos, X. (2013). Correlation of magma evolution and geophysical monitoring during the 2011-2012 El Hierro (Canary Islands) submarine eruption. *Journal of Petrology*, *54*(7), 1349–1373. https://doi.org/10.1093/petrology/egt014

Masson, D. G. (1996). Catastrophic collapse of the volcanic island of Hierro 15 ka ago and the history of landslides in the Canary Islands. *Geology*, *24*(3), 231. https://doi.org/10.1130/0091-7613(1996)024<0231:CCOTVI>2.3.CO;2

Masson, D. G., Watts, A. B., Gee, M. J. R., Urgeles, R., Mitchell, N. C., Le Bas, T. P., & Canals, M. (2002). Slope failures on the flanks of the western Canary Islands. *Earth-Science Reviews*, *57*(1–2), 1–35. https://doi.org/10.1016/S0012-8252(01)00069-1

Matzen, A. K., Baker, M. B., Beckett, J. R., & Stolper, E. M. (2011). Fe–Mg partitioning between olivine and high-magnesian melts and the nature of Hawaiian parental liquids. *Journal of Petrology*, *52*(7–8), 1243–1263. https://doi.org/10.1093/petrology/egq089

Mazza, S. E., Gazel, E., Bizimis, M., Moucha, R., Béguelin, P., Johnson, E. A., et al. (2019). Sampling the volatile-rich transition zone beneath Bermuda. *Nature*, *569*(7756), 398–403. https://doi.org/10.1038/s41586-019-1183-6

Miller, G. H., Rossman, G. R., & Harlow, G. E. (1987). The natural occurrence of hydroxide in olivine. *Physics and Chemistry of Minerals*, *14*(5), 461–472. https://doi.org/10.1007/BF00628824

Moore, J. G. (1970). Water content of basalt erupted on the ocean floor. *Contributions to Mineralogy and Petrology*, *28*(4), 272–279. https://doi.org/10.1007/BF00388949

Morimoto, N., Fabries, J., Ferguson, A. K., Ginzburg, I. V., Ross, M., Seifert, F. A., et al. (1988). Nomenclature of pyroxenes. *American Mineralogist*, *73*(9–10), 1123–1133.

Mosenfelder, J. L., & Rossman, G. R. (2013). Analysis of hydrogen and fluorine in pyroxenes: II. Clinopyroxene. *American Mineralogist*, *98*(5–6), 1042–1054. https://doi.org/10.2138/am.2013.4413

Nazzareni, S., Skogby, H., & Zanazzi, P. F. (2011). Hydrogen content in clinopyroxene phenocrysts from Salina mafic lavas (Aeolian arc, Italy). *Contributions to Mineralogy and Petrology*, *162*(2), 275–288. https://doi.org/10.1007/s00410-010-0594-z

Neave, D. A., & Putirka, K. D. (2017). A new clinopyroxene-liquid barometer, and implications for magma storage pressures under Icelandic rift zones. *American Mineralogist*, *102*(4), 777–794. https://doi.org/10.2138/am-2017-5968

Neumann, E. R., Sørensen, V. B., Simonsen, S. L., & Johnson, K. (2000). Gabbroic xenoliths from La Palma, Tenerife and Lanzarote, Canary Islands: Evidence for reactions between mafic alkaline Canary Islands melts and old oceanic crust. *Journal of Volcanology and Geothermal Research*, *103*(1–4), 313–342. https://doi.org/10.1016/S0377-0273(00)00229-8

Ni, P., Zhang, Y., & Guan, Y. (2017). Volatile loss during homogenization of lunar melt inclusions. *Earth and Planetary Science Letters*, *478*, 214–224. https://doi.org/10.1016/j.epsl.2017.09.010

Oglialoro, E., Frezzotti, M. L., Ferrando, S., Tiraboschi, C., Principe, C., Groppelli, G., & Villa, I. M. (2017). Lithospheric magma dynamics beneath the El Hierro Volcano, Canary Islands: Insights from fluid inclusions. *Bulletin of Volcanology*, *79*(10), 70. https://doi.org/10.1007/s00445-017-1152-6

Okumura, S., Nakamura, M., & Nakashima, S. (2003). Determination of molar absorptivity of IR fundamental OH-stretching vibration in rhyolitic glasses. *American Mineralogist*, *88*(11–12), 1657–1662. https://doi.org/10.2138/am-2003-11-1204

O'Leary, J. A., Gaetani, G. A., & Hauri, E. H. (2010). The effect of tetrahedral Al_3^+ on the partitioning of water between clinopyroxene and silicate melt. *Earth and Planetary Science Letters*, *297*(1–2), 111–120. https://doi.org/10.1016/j.epsl.2010.06.011

Pellicer, M. J. (1977). Estudio volcanológico de la isla de El Hierro (Islas Canarias). *Estudios Geológicos*, *33*, 181–197.

Pellicer, M. J. (1979). Estudio geoquímico del vulcanismo de la isla de Hierro. Archipiélago Canario. *Estudios Geológicos*, *35*, 11–25.

Pérez-Torrado, F. J., Rodriguez-Gonzalez, A., Carracedo, J. C., Fernandez-Turiel, J. L., Guillou, H., Hansen, A., & Rodriguez-Badiola, E. (2011). Edades C-14 del Rift ONO de El Hierro (Islas Canarias). In V. Turu & A. Constante (Eds.), *El Cuaternario en España y Áreas Afines, Avances en 2011*. Andorra: Asociación Española para el estudio de Cuaternario (AEQUA).

Peslier, A. H. (2010). A review of water contents of nominally anhydrous natural minerals in the mantles of Earth, Mars and the Moon. *Journal of Volcanology and Geothermal Research*, *197*(1–4), 239–258. https://doi.org/10.1016/j.jvolgeores.2009.10.006

Pinel, V., & Jaupart, C. (2000). The effect of edifice load on magma ascent beneath a volcano. *Philosophical Transactions of the Royal Society of London, Series A: Mathematical, Physical and Engineering Sciences*, *358*(1770), 1515–1532. https://doi.org/10.1098/rsta.2000.0601

Pinel, V., & Jaupart, C. (2004). Likelihood of basaltic eruptions as a function of volatile content and volcanic edifice size. *Journal of Volcanology and Geothermal Research*, *137*(1–3), 201–217. https://doi.org/10.1016/j.jvolgeores.2004.05.010

Pinel, V., & Jaupart, C. (2005). Some consequences of volcanic edifice destruction for eruption conditions. *Journal of Volcanology and Geothermal Research*, *145*(1–2), 68–80. https://doi.org/10.1016/j.jvolgeores.2005.01.012

Putirka, K. D. (2008). Thermometers and barometers for volcanic systems. *Reviews in Mineralogy and Geochemistry*, *69*(1), 61–120. https://doi.org/10.2138/rmg.2008.69.3

Putirka, K. D., Johnson, M., Kinzler, R., Longhi, J., & Walker, D. (1996). Thermobarometry of mafic igneous rocks based on clinopyroxene-liquid equilibria, 0-30 kbar. *Contributions to Mineralogy and Petrology*, *123*(1), 92–108. https://doi.org/10.1007/s004100050145

Putirka, K. D., Mikaelian, H., Ryerson, F., & Shaw, H. (2003). New clinopyroxene-liquid thermobarometers for mafic, evolved, and volatile-bearing lava compositions, with applications to lavas from Tibet and the Snake River Plain, Idaho. *American Mineralogist*, *88*(10), 1542–1554. https://doi.org/10.2138/am-2003-1017

Radu, I. B., Skogby, H., Troll, V. R., Deegan, F. M., Geiger, H., Müller, D., & Thordarson, T. (2023). Water in clinopyroxene from the 2021 Geldingadalir eruption of the Fagradalsfjall Fires, SW-Iceland. *Bulletin of Volcanology*, *85*(5), 31. https://doi.org/10.1007/s00445-023-01641-4

Ranero, C. R., Torne, M., & Banda, E. (1995). Gravity and multichannel seismic reflection constraints on the lithospheric structure of the Canary Swell. *Marine Geophysical Researches*, *17*(6), 519–534. https://doi.org/10.1007/BF01204342

Rivera, J., Lastras, G., Canals, M., Acosta, J., Arrese, B., Hermida, N., et al. (2013). Construction of an oceanic island: Insights from the El Hierro (Canary Islands) 2011-2012 submarine volcanic eruption. *Geology*, *41*(3), 355–358. https://doi.org/10.1130/G33863.1

Rodriguez-Badiola, E., Pérez-Torrado, F. J., Carracedo, J. C., & Guillou, H. (2006). *Petrografía y geoquímica del edifico volcánico Teide-Pico Viejo y las dorsales noreste y noroeste de Tenerife*. Ministerio de Medio Ambiente, Organismo Autónomo Parques Nacionales.

Roeder, P. L., & Emslie, R. F. (1970). Olivine-liquid equilibrium. *Contributions to Mineralogy and Petrology*, *29*(4), 275–289. https://doi.org/10.1007/BF00371276

Schmincke, H. U. (1982). Volcanic and chemical evolution of the Canary Islands. In U. Von Rad, K. Hinz, M. Sarnthein, & E. Seibold (Eds.), *Geology of the northwest African continental margin* (pp. 273–306). Springer Berlin Heidelberg. https://doi.org/10.1007/978-3-642-68409-8_12

Sides, I. R., Edmonds, M., Maclennan, J., Swanson, D. A., & Houghton, B. F. (2014). Eruption style at Kīlauea Volcano in Hawai'i linked to primary melt composition. *Nature Geoscience*, *7*(6), 464–469. https://doi.org/10.1038/ngeo2140

Simons, K., Dixon, J., Schilling, J. G., Kingsley, R., & Poreda, R. (2002). Volatiles in basaltic glasses from the Easter-Salas y Gomez Seamount Chain and Easter Microplate: Implications for geochemical cycling of volatile elements. *Geochemistry, Geophysics, Geosystems*, *3*(7), 1–29. https://doi.org/10.1029/2001GC000173

Skogby, H. (1994). OH incorporation in synthetic clinopyroxene. *American Mineralogist*, *79*(3–4), 240–249.

Skogby, H. (2006). Water in natural mantle minerals I: Pyroxenes. *Reviews in Mineralogy and Geochemistry*, *62*(1), 155–167. https://doi.org/10.2138/rmg.2006.62.7

Spaans, K., Hreinsdóttir, S., Hooper, A., & Ófeigsson, B. G. (2015). Crustal movements due to Iceland's shrinking ice caps mimic magma inflow signal at Katla volcano. *Scientific Reports*, *5*(1), 10285. https://doi.org/10.1038/srep10285

Stroncik, N. A., Klügel, A., & Hansteen, T. H. (2009). The magmatic plumbing system beneath El Hierro (Canary Islands): Constraints from phenocrysts and naturally quenched basaltic glasses in submarine rocks. *Contributions to Mineralogy and Petrology*, *157*(5), 593–607. https://doi.org/10.1007/s00410-008-0354-5

Sundvall, R., & Stalder, R. (2011). Water in upper mantle pyroxene megacrysts and xenocrysts: A survey study. *American Mineralogist*, *96*(8–9), 1215–1227. https://doi.org/10.2138/am.2011.3641

Taracsák, Z., Hartley, M. E., Burgess, R., Edmonds, M., Iddon, F., & Longpré, M. A. (2019). High fluxes of deep volatiles from ocean island volcanoes: Insights from El Hierro, Canary Islands. *Geochimica et Cosmochimica Acta*, *258*, 19–36. https://doi.org/10.1016/j.gca.2019.05.020

Tenzer, R., Bagherbandi, M., & Vajda, P. (2013). Global model of the upper mantle lateral density structure based on combining seismic and isostatic models. *Geosciences Journal*, *17*(1), 65–73. https://doi.org/10.1007/s12303-013-0009-z

Tian, Z. Z., Liu, J., Xia, Q. K., Ingrin, J., Hao, Y. T., & Christophe, D. (2017). Water concentration profiles in natural mantle orthopyroxenes: A geochronometer for long annealing of xenoliths within magma. *Geology*, *45*(1), 87–90. https://doi.org/10.1130/G38620.1

Ubide, T., Larrea, P., Becerril, L., & Galé, C. (2022). Volcanic plumbing filters on ocean-island basalt geochemistry. *Geology*, *50*(1), 26–31. https://doi.org/10.1130/G49224.1

Von Aulock, F. W., Kennedy, B. M., Schipper, C. I., Castro, J. M., E. Martin, D., Oze, C., et al. (2014). Advances in Fourier transform infrared spectroscopy of natural glasses: From sample preparation to data analysis. *Lithos*, *206–207*, 52–64. https://doi.org/10.1016/j.lithos.2014.07.017

Wade, J. A., Plank, T., Hauri, E. H., Kelley, K. A., Roggensack, K., & Zimmer, M. (2008). Prediction of magmatic water contents via measurement of H2O in clinopyroxene phenocrysts. *Geology*, *36*(10), 799–802. https://doi.org/10.1130/G24964A.1

Wallace, P. J. (1998a). Pre-eruptive H_2O and CO_2 contents of mafic magmas from the submarine to emergent shield stages of Gran Canaria. *Ocean Drilling Program*, *157*, 411–420. https://doi.org/10.2973/odp.proc.sr.157.146.1998

Wallace, P. J. (1998b). Water and partial melting in mantle plumes: Inferences from the dissolved H_2O concentrations of Hawaiian basaltic magmas. *Geophysical Research Letters*, *25*(19), 3639–3642. https://doi.org/10.1029/98GL02805

Walter, T. R., Troll, V. R., Cailleau, B., Belousov, A., Schmincke, H. U., Amelung, F., & van den Bogaard, P. (2005). Rift zone reorganization through flank instability in ocean island volcanoes: An example from Tenerife, Canary Islands. *Bulletin of Volcanology*, *67*(4), 281–291. https://doi.org/10.1007/s00445-004-0352-z

Weis, F. A., Skogby, H., Troll, V. R., Deegan, F. M., & Dahren, B. (2015). Magmatic water contents determined through clinopyroxene: Examples from the western Canary Islands, Spain. *Geochemistry, Geophysics, Geosystems*, *16*(7), 2127–2146. https://doi.org/10.1002/2015GC005800

Weis, F. A., Stalder, R., & Skogby, H. (2016). Experimental hydration of natural volcanic clinopyroxene phenocrysts under hydrothermal pressures (0.5–3 kbar). *American Mineralogist*, *101*(10), 2233–2247. https://doi.org/10.2138/am-2016-5711CCBYNCND

Withers, A. C., Bureau, H., Raepsaet, C., & Hirschmann, M. M. (2012). Calibration of infrared spectroscopy by elastic recoil detection analysis of H in synthetic olivine. *Chemical Geology*, *334*, 92–98. https://doi.org/10.1016/j.chemgeo.2012.10.002

Woods, S. C., Mackwell, S., & Dyar, D. (2000). Hydrogen in diopside: Diffusion profiles. *American Mineralogist*, *85*(3–4), 480–487. https://doi.org/10.2138/am-2000-0409

Zaczek, K., Troll, V. R., Cachao, M., Ferreira, J., Deegan, F. M., Carracedo, J. C., et al. (2015). Nannofossils in 2011 El Hierro eruptive products reinstate plume model for Canary Islands. *Scientific Reports*, *5*(1), 7945. https://doi.org/10.1038/srep07945

References From the Supporting Information

Ferguson, D. J., Gonnermann, H. M., Ruprecht, P., Plank, T., Hauri, E. H., Houghton, B. F., & Swanson, D. A. (2016). Magma decompression rates during explosive eruptions of Kīlauea volcano, Hawaii, recorded by melt embayments. *Bulletin of Volcanology*, *78*(10), 71. https://doi.org/10.1007/s00445-016-1064-x

Lloyd, A. S., Ruprecht, P., Hauri, E. H., Rose, W., Gonnermann, H. M., & Plank, T. (2014). NanoSIMS results from olivine-hosted melt embayments: Magma ascent rate during explosive basaltic eruptions. *Journal of Volcanology and Geothermal Research*, *283*, 1–18. https://doi.org/10.1016/j.jvolgeores.2014.06.002